4.0 Parameter dependencies and application of the derived atomic data relevant to neutral deuterium beam attenuation and emission

4.1 Introduction

There are two methods which can be employed to determine the neutral deuterium beam density as a function of penetration depth into a tokamak plasmas, see chapter 1.0. The first is a numerical attenuation calculation, which requires theoretical effective stopping coefficients. The second and more accurate method, involves the use of Balmer-alpha beam emission spectroscopy and requires theoretical effective emission coefficients. In this chapter we explore the parameter dependencies of the effective stopping and Balmer-alpha emission coefficients. Particular emphasis is placed on identifying the underlying atomic processes which contribute to both of these coefficients. We then consider the practical method of archiving such data and assembling effective coefficients for a composite plasma. The effective coefficients presented in this chapter have been calculated in a bundled-nS picture up to n=110 using ADAS310.

4.2 Effective collisional-radiative ionisation coefficients

In the following sub-sections we show the primary parameter dependencies of the collisional-radiative ionisation coefficients. The collisional-radiative ionisation coefficient is usually referred to as the effective beam stopping coefficient in fusion beam studies, where it describes the rate at which the beam neutrals are ionised as the beam traverses the plasma. Figure 4.1 shows the general behaviour of the effective stopping coefficient as a function of electron density and neutral beam energy for a deuterium beam penetrating into a pure D^+ plasma. The parameters to which the effective beam stopping coefficient is most sensitive include the electron density, the neutral beam energy, plasma temperature and the nuclear charge of fully stripped plasma impurity ions. It should be noted that the collisional-radiative ionisation coefficient is also strongly dependent on the ion density, in the present work however the coefficients are calculated in terms of the electron density with charge neutrality imposed.

We also wish to achieve two further objectives. Firstly we want to show the importance of including the influence of all the impurities contained in a composite plasma while evaluating effective stopping coefficients. To achieve this we evaluate the effective coefficients using ADAS310 for a range of composite plasmas and identify the individual contributions due to each impurity ion. We emphasise however that it is common practise to assemble composite coefficients using the rapid look up tables as discussed in section 4.4. Secondly we want to illustrate the sensitivity of the effective beam stopping coefficient following small changes in the fundamental atomic data which enters into the modelling as input.

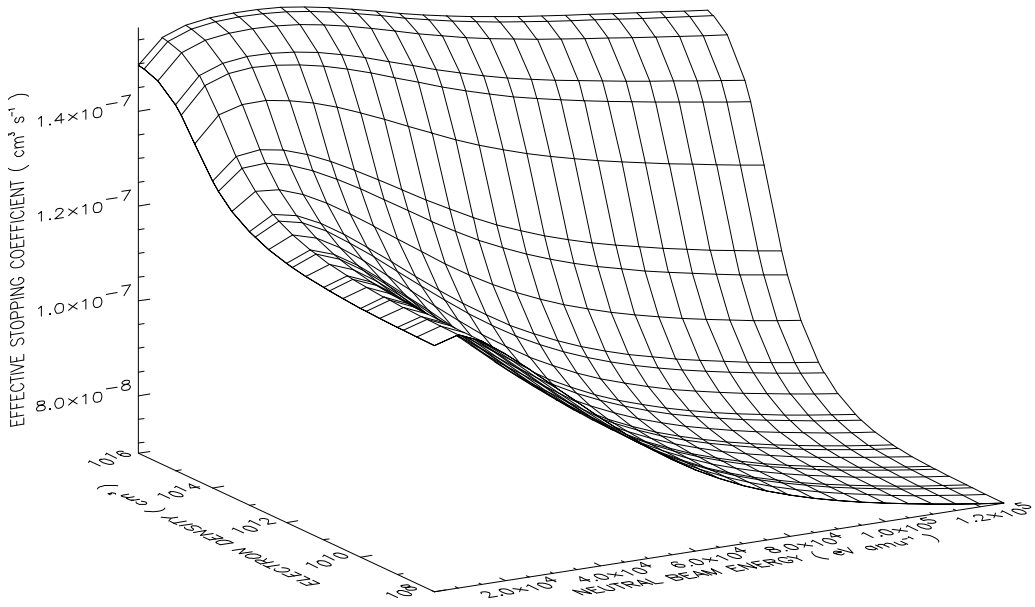

Figure 4.1 A surface plot of the effective stopping coefficient for a pure deuterium plasma with a temperature of 2×10^3 eV. Near the coronal limit at 1×10^8 cm^{-3}, the behaviour of the stopping coefficient reflects the rate coefficients for direct ionisation from the ground state of the beam neutrals via charge exchange and ion impact ionisation. As the density is increased the collisional losses from the excited states increases until a high density limit is reached.

4.2.1 Density dependence

The electron and ion density both control the effectiveness at which the atomic processes contribute to the beam stopping coefficient. Due to the efficiency of ion collisions the ion density is more influential. In figure 4.2 the influence of the

electron density on the effective stopping coefficient can be observed as a function of beam energy.

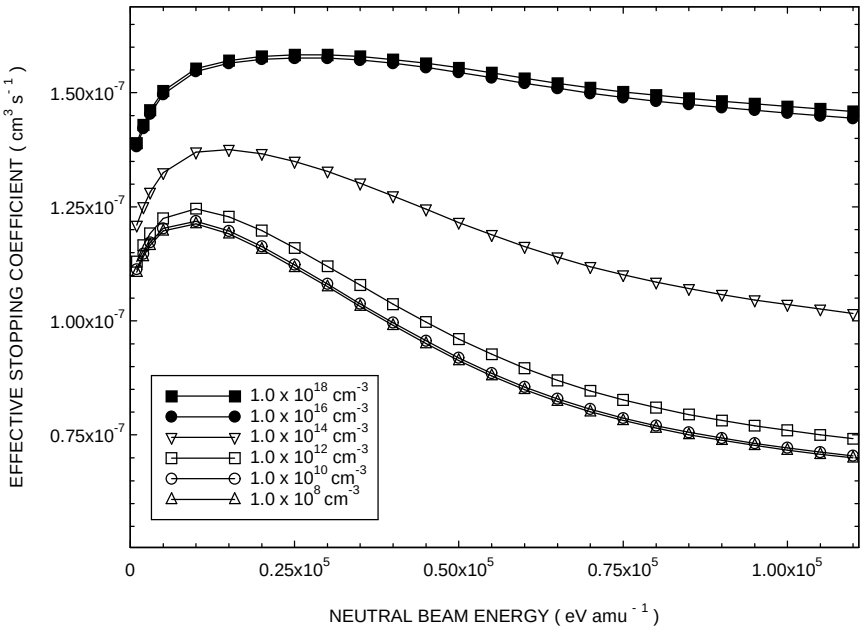

Figure 4.2 Effective beam stopping coefficient Vs neutral beam energy for a pure D^+ plasma. The ion temperature is 2×10^3 eV. The density dependence of the effective coefficient is clearly illustrated with the assistance of the low and high density limit.

As can be seen in figure 4.2, the departure from the low density coronal limit appears around ~10^{10} cm^{-3}, while the formation of the high density limit is approached at ~1 x 10^{18} cm^{-3}. The characteristic density dependence of the stopping coefficient is not only confined to a pure D^+ plasma. We have undertaken similar behavioural studies for a wide range of plasmas with a different impurity content. As an extreme example we show in figure 4.3 the density dependence of the effective stopping coefficient for a deuterium beam penetrating into a hypothetical plasma of pure C^{6+}. We should emphasise that it is the ion density which governs the behaviour of the effective stopping coefficient even though we show the behaviour of the effective coefficient in terms of the electron density.

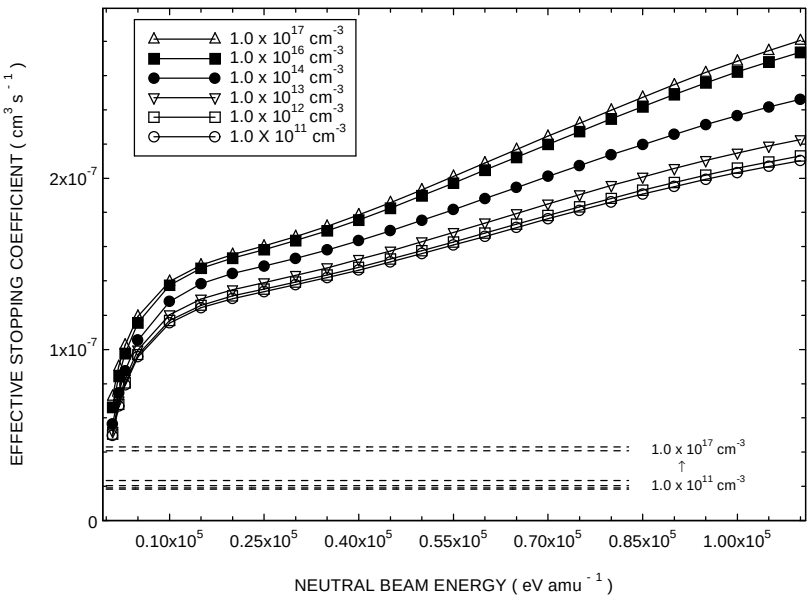

Figure 4.3 Beam stopping coefficient Vs the neutral beam energy for a hypothetical plasma of pure C^{6+} . The ion temperature is 2 x 10^3 eV. Also shown in the figure, with the dashed lines, is the contribution to the effective coefficient due to electron collision for a range of electron densities.

The low density coronal limit can be observed to form around ~1.0 x 10^{11} cm^{-3}, which corresponds to an ion density of ~1.6 x 10^{10} cm^{-3}, while the high density picture occurs at an electron density of ~1.0 x 10^{17} cm^{-3}. Also shown in the figure, with the dashed lines, is the contribution to the effective stopping coefficient due to electrons collisions. The electrons are moving at such great speeds that their small contribution is independent of the beam energy. It is of interest to point out the difference in the magnitude of the stopping coefficient for a pure D^+ and C^{6+} plasma. The latter is substantial larger and is due to the greater efficiency of the C^{6+} plasma ions at stripping the electrons from the beam atoms. The influence of the nuclear charge of the plasma impurity ions is discussed in 4.2.4.

4.2.2 Neutral beam energy dependence

The neutral beam energy governs the relative efficiency of electrons and ions causing the attenuation and population redistribution of the neutral beam atoms. However the extent of the energy dependence of the effective stopping coefficient is also

coupled to the ion density. In figure 4.4 we illustrate the influence of the neutral beam energy on the stopping coefficient as a function of electron density for a pure D^+ plasma.

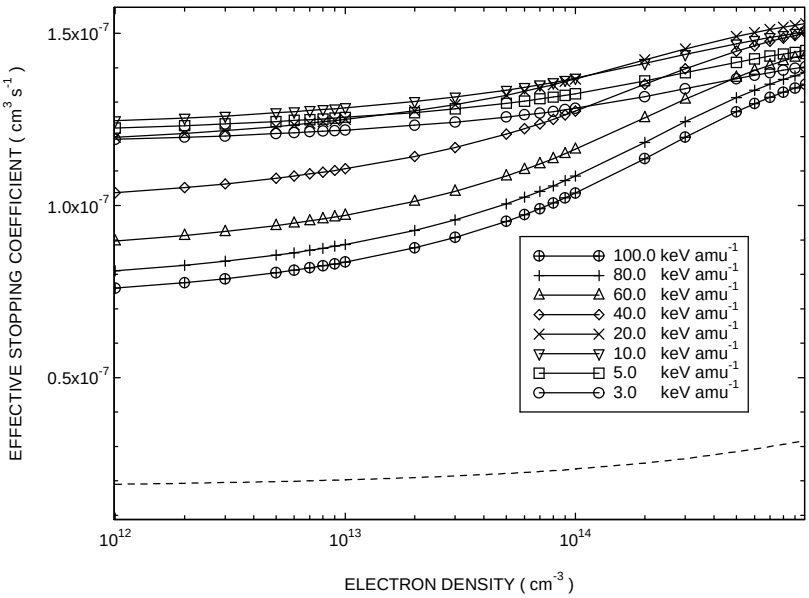

Figure 4.4 A plot of the effective stopping coefficient Vs electron density for a pure D^+ plasma. The influence of the neutral beam energy on the effective stopping coefficient for a fixed ion temperature of 2 x 10^3 eV is shown. Also shown, with the dashed line, is the small contribution to the effective stopping coefficient due to electron collisions.

It can be seen that for a fixed beam energy the effective stopping coefficient increases as the electron density is increased. This is due to the role of stepwise atomic processes which become important as the electron and hence the ion density is increased. Also shown, with the dashed line, is the small contribution to the effective stopping coefficient due to electron collisions. The contribution due to electrons also increases as the electron density is increased. However the rate of increase is substantially smaller since collisional redistribution due to electron collision is less efficient. It can also be observed in figure 4.4, that for a fixed electron density the effective stopping coefficient increases and then decreases as the beam energy is increased from 3.0 to 100 keV amu^{-1}. This simply reflects the energy dependence of the underlying atomic processes, see chapter 2.0. The net effect of all the competing processes is that the effective stopping coefficient can be observed to increase and then slowly decrease as a function of beam energy.

4.2.3 Temperature dependence

The plasma temperature dependence of the stopping coefficient arises from the relative collision velocities between the beam atoms and the fully stripped thermal plasma ions. The relative collision velocities govern the behaviour of the collision cross sections which in turn influence the rate coefficients which enter into the statistical balance equations. In the simplest form, the expression for the rate coefficient for an arbitrary process is given as,

$$\langle \sigma v \rangle = \int_{v_{\min}}^{\infty} |v_r| f(v_t) \sigma(|v_r|) dv_t \qquad 4.1$$

where $f(v_t)$ is the velocity distribution of the thermal plasma ions, $\sigma(|v_r|)$ is the collision cross section and v_r is the relative collision velocity between the beam atoms and the thermal ions, i.e. $|v_r|=|v_b-v_t|$.

In the case where the beam velocity, v_b, is substantially greater than the thermal velocity of the plasma ions, it can be shown that the rate coefficients and hence the effective beam stopping coefficients are independent of the plasma temperature. The temperature dependence of the stopping coefficients can only be observed when the beam velocity is not vastly different from the thermal velocity of the plasma ions. In such circumstances, an increase or decrease in the plasma temperature alters the relative collision velocity as well as the shape and position of the velocity distribution. Depending on the behaviour of the underlying collision cross sections this may result in either increasing or decreasing the effective stopping coefficient. When the beam velocity is slightly greater than the thermal velocity of the plasma ions, an increase in the plasma temperature contributes to decreasing the relative collision velocity. In figure 4.5 we show the temperature dependence of the stopping coefficient as a function of beam energy for such a scenario.

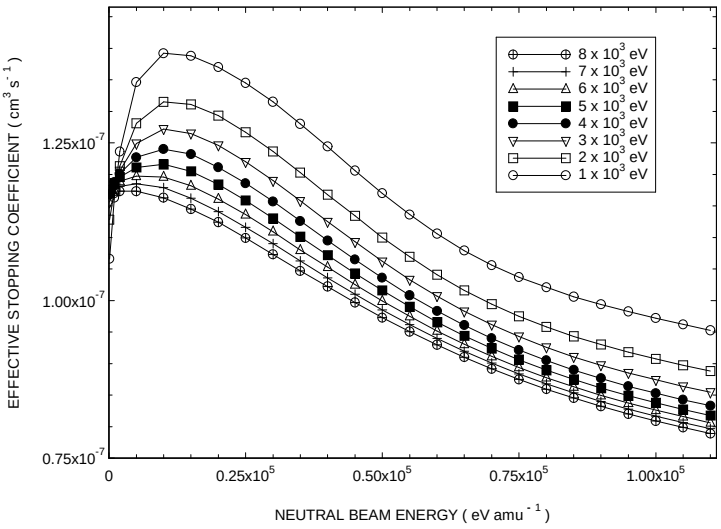

Figure 4.5 A plot of the effective stopping coefficient Vs neutral beam energy for a pure D^+ plasma with a density of 3.0×10^{13} cm^{-3}.

As the plasma temperature increases, it can be observed from figure 4.5 that the effective stopping coefficient decreases. This is attributed to the fact that as the relative collision velocity decreases the collision cross sections also decrease. It is of interest to point out that when the thermal velocity of the plasma ions is slightly greater than the beam velocity the opposite occurs. As the plasma temperature increases the relative collision velocity and the collision cross sections also increase, see figure 4.6.

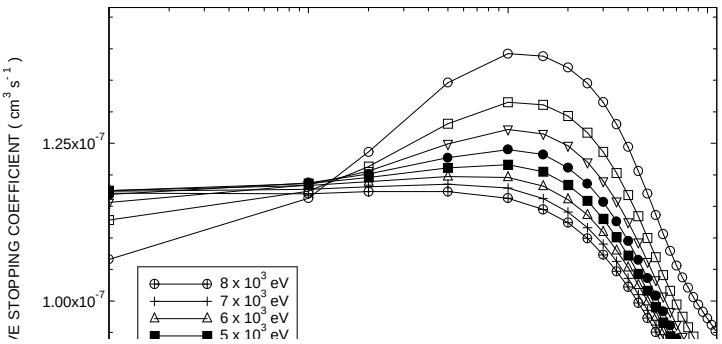

Figure 4.6 Beam stopping coefficient Vs neutral beam energy for D^+ plasma with a density of 3.0×10^{13} cm^{-3}. In the low energy regime an increase in the plasma temperature results in an increase in the effective stopping coefficient.

In the low energy regime of figure 4.6, as the plasma temperature increases the effective stopping coefficients also increase. It should be noted that an increase or decrease in the relative collision velocity does not necessary result in a similar increase or decrease in the effective stopping coefficient. The influence of the relative collision velocity depends on the behaviour of the collision cross sections. Nevertheless the temperature dependence of the stopping coefficient is weak and is almost independent of the beam energy and the electron density. As illustrated in figure 4.5 and 4.6, increasing the temperature by a factor of 5 only results in an average change of 12 % in the effective stopping coefficient.

4.2.4 Nuclear charge dependence

The nuclear charge of a fully stripped plasma ion characterises how effective the ion will be at ionising the neutral beam atoms. As the nuclear charge increases, the associated cross sections which describe the behaviour of charge exchange and ion impact ionisation also increase, see chapter 2.0. In this section we briefly illustrate the influence of fully stripped plasma ions on the effective stopping coefficient. We show in figure 4.7, the effective stopping coefficient as a function of beam energy for a variety of pure impurity plasmas.

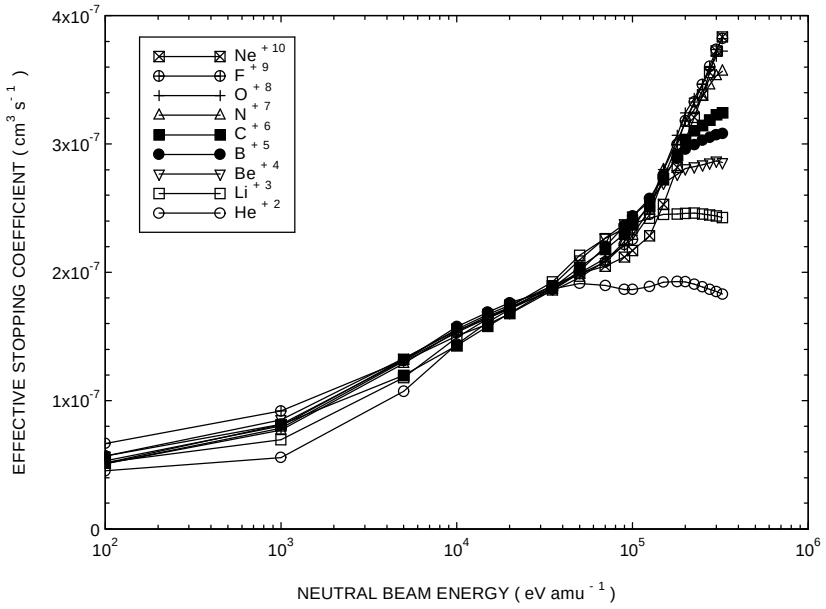

Figure 4.7 Beam stopping coefficient Vs neutral beam energy for a pure impurity plasma. Note the asymptotic behaviour of the beam stopping coefficient for each impurity. The electron density was 3.0 x 10^{13} cm^{-3} and the plasma temperature was 2.0 x 10^3 eV.

In the low energy regime we can observe a charge dependence of the effective stopping coefficient. This is simply due to the behaviour of the underlying charge exchange cross sections. The charge exchange cross sections scale approximately with the nuclear charge of the receiver ion. As the beam energy is increased a near coincidence of curves in the relevant beam range of current tokamaks can be observed. Finally in the high energy regime, the charge dependence of the effective stopping coefficient can again be observed. On this occasion however it is due to the charge dependence of the ion impact ionisation cross sections. The ion impact ionisation cross sections also scale approximately with the nuclear charge of the impurity ion. From the results shown in figure 4.7, it would appear that the effective stopping coefficient also scales approximately with the nuclear charge. However the electron density was fixed at a value of 3.0×10^{13} cm^{-3} and charge neutrality had been imposed. Therefore as the nuclear charge of the plasma ion increased, the corresponding number density decreased. Therefore the behaviour of the effective stopping coefficient in fact scales with a value which is slightly larger than the nuclear charge .

4.2.5 The importance of impurities

So far we have presented data showing the primary parameter dependencies of the effective stopping coefficients for pure plasmas. Working fusion plasmas consist of electrons and deuterons together with unavoidable small concentrations of various fully stripped impurity species. The different components which make up the composition of the plasma all contribute to exciting and ionising a penetrating beam. In this sub-section we attempt to illustrate the influence of such mixed impurities while evaluating effective stopping coefficients. This allows one to quantitatively assess the importance of considering the mixed impurity content of the plasma. The approach taken was to evaluate effective stopping coefficients for a range of composite plasma and in each case highlight the individual contribution from each impurity contained in the plasma.

We begin by considering a simple plasma which consists of 98 % D^+ and 2 % He^{2+}. In figure 4.8 we show the energy and density dependence of the effective

stopping coefficient, also shown in both figures are the individual contributions due to each ion.

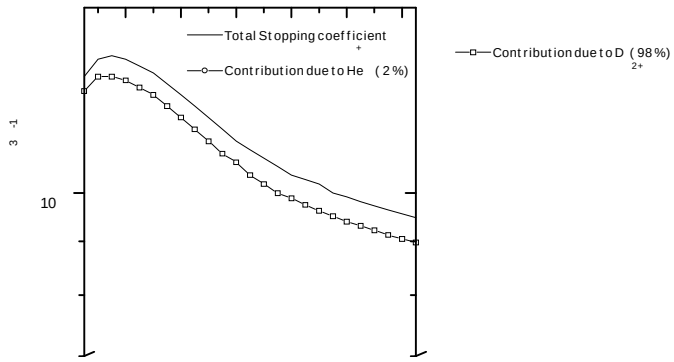

Figure 4.8 A plot of the effective beam stopping coefficient for a composite plasma consisting of 98% D^+ and 2 % He^{2+}. The plot on the left exhibits the energy dependence of the effective stopping coefficient while the plot on the right illustrates the density dependence. The ion temperature was 2.0 x 10^3 eV and the electron density for the plot on the left was 3.0 x 10^{13} cm^{-3}. The beam energy corresponding to the plot on the right was 5.0 keV amu^{-1}.

If we first consider the energy dependence of the composite stopping coefficient which is shown in the plot on the left of figure 4.8. It can be observed that the contribution to the total stopping coefficient due to the 2% concentration of He^{2+}, increases from 2.5 % at 5.0 keV amu^{-1} to 5.3 % at 120.0 keV amu^{-1}. The contribution due to the He^{2+} ions is in fact greater than their total concentration in the plasma. This simply reflects the larger cross sections associated with He^{2+} ions and hence their greater efficiency at stripping electrons from the beam atoms in comparison with the D^+ ions. This effect can also be observed in the plot on the right in figure 4.8, which illustrates the electron density dependence of the composite stopping coefficient. At a density of 1.0 x10^{12} cm^{-3} the contribution due to He^{2+} is 5.69 %, which decreases to a value of 4.81 % as the electron density is increased.

We now consider a slightly different plasma which consists of 96 % D^+, 2% He^{2+} and 2% Be^{4+}. The energy and density dependence of the composite stopping coefficient can be seen in figure 4.9.

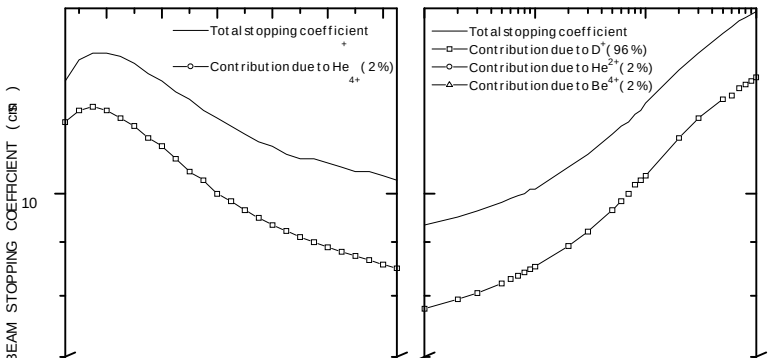

Figure 4.9 A plot of the effective beam stopping coefficient for a composite plasma consisting of 96% D^+, 2% He^{2+} and 2% Be^{4+}. The plot on the left shows the energy dependence of the composite coefficient while the plot on the right exhibits the density dependence. The ion temperature was 2.0 x 10^3 eV and the electron density for the plot on the left was 3.0 x 10^{13} cm^{-3}. The beam energy for the plot on the right was 5.0 keV amu^{-1}.

As shown in the plot on the left of figure 4.9, the contribution to the total stopping coefficient due to the He^{2+} ions increases from 2.41 to 4.66 % at the respective beam energies of 5.0 and 120.0 keV amu^{-1}. The corresponding contributions due to the Be^{4+} ions is 6.31 and 12.78 %. The larger contribution due to the Be^{4+} ions is due to the increase in the associated charge exchange and ion impact ionisation cross sections. The increase in the cross sections is so great that the decrease in the number density of Be^{4+} ions in comparison to the He^{2+} ions, since charge neutrality is imposed, has little effect. If we now consider the electron density dependence of the composite stopping coefficient which is shown in the plot on the right in figure 4.9. It can be seen that at a density of 1.0 x 10^{12} cm^{-3}, the contributions to the total stopping coefficient due to the He^{2+} and Be^{4+} ions are respectively 5.1 and 11.67 %. The

contribution due to each ion decreases as the electron density is increased. This reflects the increased contribution due to the D^+ ions as a result of stepwise atomic processes. At a density of 1.0 x 10^{15} cm^{-3}, the contribution due to He^{2+} and Be^{4+} ions are now respectively 4.45 and 9.32%.

The final plasma which is under scrutiny consists of 93 % D^+, 2% He^{2+}, 2% Be^{4+} and 3% C^{6+}. The energy and density dependence of the composite stopping coefficient and the associated contributions from each ion is shown in figure 4.10.

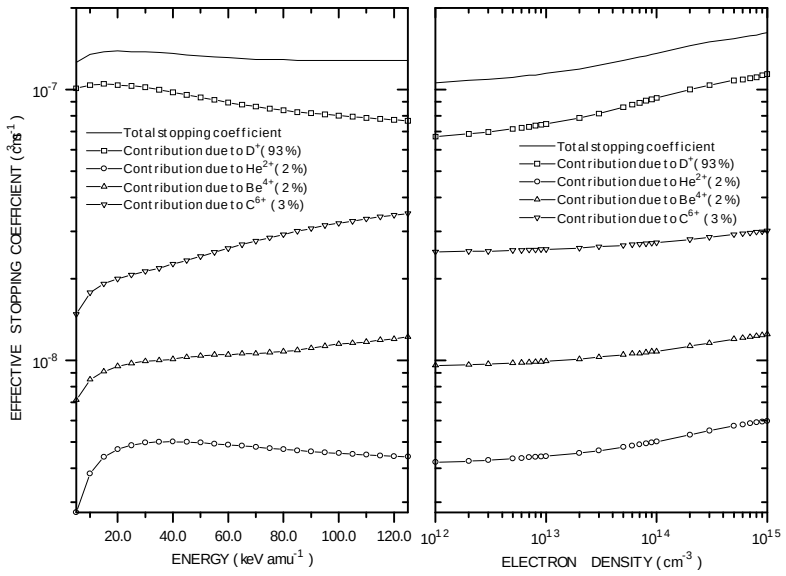

Figure 4.10 A plot of the effective beam stopping coefficient for a composite plasma consisting of 93 % D^+, 2% He^{2+}, 2% Be^{4+} and 3% C^{6+}. The plot on the left shows the energy dependence while the plot on the right exhibits the electron density dependence. The plasma temperature was 2.0 x 10^3 eV and the electron density for the plot on the left was 3.0 x 10^{13} cm-3. The neutral beam energy for the plot on the right was 5.0 keV amu^{-1} .

The energy dependence of the composite stopping coefficient and the contributions from each ion are shown in the plot on the left of figure 4.10. It can be seen that at 5.0 keV amu^{-1}, the contributions to the total stopping coefficients due to the He^{2+} , Be^{4+} and C^{6+} ions are respectively 2.18, 5.67 and 11.74 %. These contributions can be observed to increase and reach a maximum of 3.44 %, 9.53 % and 27.26 % at 125 keV amu^{-1}. It is some what surprising that a mere 3 % concentration of C^{6+} can contribute as much as 27.26 % to the total stopping coefficient. This is due to the

large cross sections associated with the C^{6+} ions. Similar results can be seen in the plot on the right in figure 4.10, which illustrates the electron density dependence of the composite stopping coefficient.

4.2.6 Influence of fundamental low level data

In this sub-section we probe the influence of the fundamental atomic data on the effective stopping coefficients. The approach taken here was to modify the cross sections for each of the atomic processes individually, and then investigate what effect it had on the stopping coefficient. Since ion-atom collisions dominate the population redistribution and attenuation, we have restricted ourselves to modifying only the ion-atom collision database. For convenience we only consider a pure D^+ plasma.

We begin by first assessing the implications of increasing the cross sections which describe the behaviour of direct charge exchange and ion impact ionisation by 10 %. The results can be seen in figure 4.11, where we show the effective stopping coefficient as a function of beam energy for three different electron densities. The electron densities were selected to correspond to the coronal, collisional-radiative and high density picture. Also shown in the figure are the results obtained from the unmodified ion-atom collision database.

In the low density coronal picture, it can be observed from figure 4.11 that a 10 % change in the cross sections results in an increase in the stopping coefficient by 8.54 % at 3.0 keV amu^{-1}, which then increases slightly and then decreases to 7.29 % at 120.0 keV amu^{-1}. Due to processes which counter direct charge exchange and ion impact ionisation a change of 10 % in the fundamental data does not give rise to a 10 % change in the effective stopping coefficient. An example of such a process would be collisional excitation, which contributes to depopulating the ground state without ionising the beam atoms and hence reducing the influence of such direct processes. The evidence to suggest this can be seen when the electron density is increased. At an electron density of 3.0×10^{13} cm^{-3}, the influence of the modified data results in a change of 8.06 % at 3.0 keV amu^{-1}, which then decreases to 5.85 % at 120.0 keV amu^{-1}. The increase in the density has enhanced the influence of collisional excitation

and stepwise atomic processes, which in turn reduces the influence of the fundamental data for direct charge exchange and impact ionisation. At an electron density of 1.0 x 10^{15} cm^{-3} the result of modifying the cross sections is now only 7.14 % at 3.0 keV amu^{-1} and 3.78 % at 120.0 keV amu^{-1}.

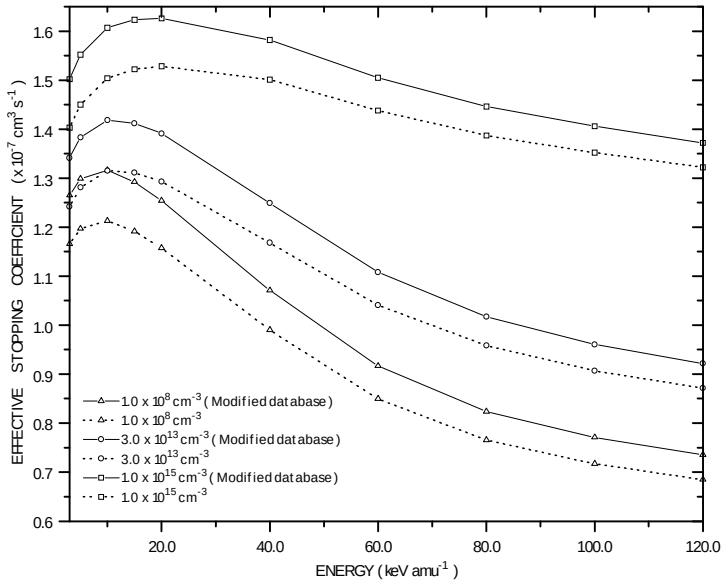

Figure 4.11 Effective stopping coefficient Vs the neutral beam energy for a range of electron densities. The electron densities were selected to correspond to the coronal, collisional-radiative and high density picture. The dashed lines represent the results obtained from the unmodified database. The solid lines represent the results obtained by increasing the direct charge exchange and ion impact ionisation cross-sections by 10 %. The ion temperature was 2.0 x 10^3 eV.

It is of interest to identify which of the atomic processes associated with the ground state has the most significant effect on the stopping coefficient. In figure 4.12 we show the results of individually modifying the direct charge exchange and ion impact ionisation cross sections by 10 %.

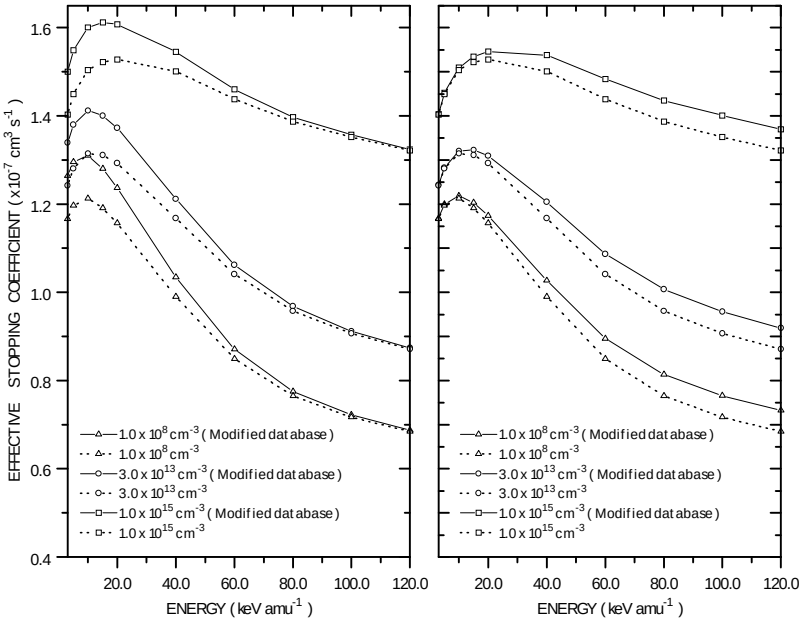

Figure 4.12 Effective stopping coefficient Vs the neutral beam energy for a pure D^+ plasma. The dashed lines are the results from the unmodified database. The solid lines are the results obtained from the modified database. The plot on the left shows the results of increasing the direct charge exchange cross section by 10%. The plot to the right shows the effect of increasing the direct ion impact ionisation cross section by 10 %.

If we first consider the plot on the left in figure 4.12. In this plot the results of changing the direct charge exchange cross section can be observed as a function of beam energy for three different electron densities. At an electron density of 1.0 x10^8 cm^{-3}, it can be observed that the modified data has resulted in the effective stopping coefficient differing substantially in the low energy regime. However as the beam energy is increased the difference becomes less significant and eventually the results from the modified and unmodified data agree. An increase in the effective stopping coefficient by 7.69 % can be seen at 3.0 keV amu^{-1}, however at 60.0 keV amu^{-1} it is only 2.47 % and at 120 keV amu^{-1} it is now just 0.43 %. If we increase the electron density the difference between the modified and unmodified data decrease in the same manner as show in figure 4.11. The influence of the charge exchange data is as expected. It is interesting to point out that in figure 4.11 a difference of 8.54 % was observed at a density of 1.0 x 10^8 cm^{-3} , therefore we can infer that the contribution

due to altering the ion impact ionisation cross section by 10 % is only 0.85 % at 3.0 keV amu^{-1}. If we now focus on the plot on the right in figure 4.12. This plot contains the results of modifying the direct ion impact ionisation cross section by 10%. As can be observed for an electron density of 1.0 x 10^{8} cm^{-3}, as the beam energy increases the influence of the modified data also increases. At an energy of 3.0 keV amu^{-1} the influence is negligible, however at an energy of 60.0 keV amu^{-1} an increase in the effective coefficient by 5.41 % can be seen, which increases further to reach a value of 7.0 % at 120.0 keV amu^{-1}. As before, an increase in the electron density enhances stepwise atomic processes, which reduces the influence of modifying the direct cross sections.

We now consider the implications of modifying the ion impact excitation cross sections. The ion-atom collision database contain ion impact excitation cross sections from the ground state to the n=2,3,4 and n=5 shell. In figure 4.13 we show the results of modifying all of the ion impact excitation cross sections by 20%.

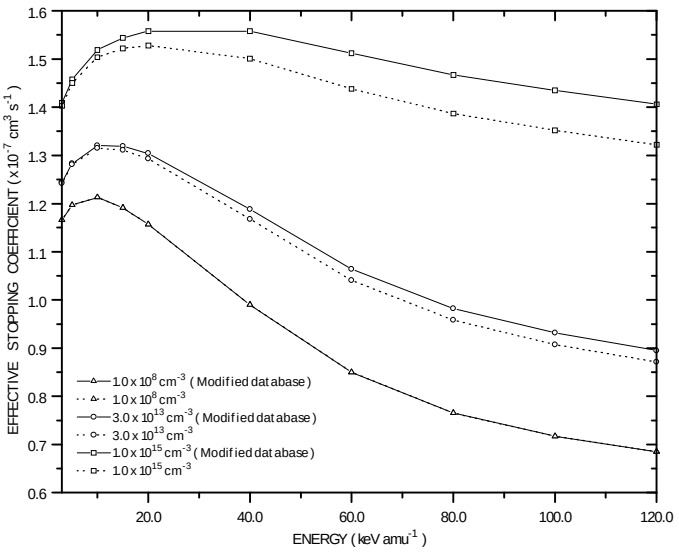

Figure 4.13 Effective stopping coefficient Vs the neutral beam energy for a range of electron densities. The ion temperature was 2.0 x 10^{3} eV. The dashed lines represent the results from the unmodified database. The solid lines are the results obtained by modifying the ion impact excitation cross sections by 20 %.

In the low density regime, the influence of modifying the fundamental data is negligible. As the electron density is increased the influence of the modified data becomes more significant, even though it is still small. At an electron density of 3.0 x 10^{13} cm^{-3}, the difference between the effective stopping coefficient calculated with and without the modified data, increases as the beam energy also increases. At a beam energy of 20.0 keV amu^{-1}, the difference is only 0.77 % which increases to 2.75 % at 120.0 keV amu^{-1}. Even at 1.0 x 10^{15} cm^{-3} , the largest difference which can be observed is 6.81 % at 120.0 keV amu^{-1}. In figure 4.14 we show the results of individually changing the ion impact excitation cross sections, we have refrained from showing the results for the excitation cross section from the ground state to the n=5 shell, since the effect was insignificant.

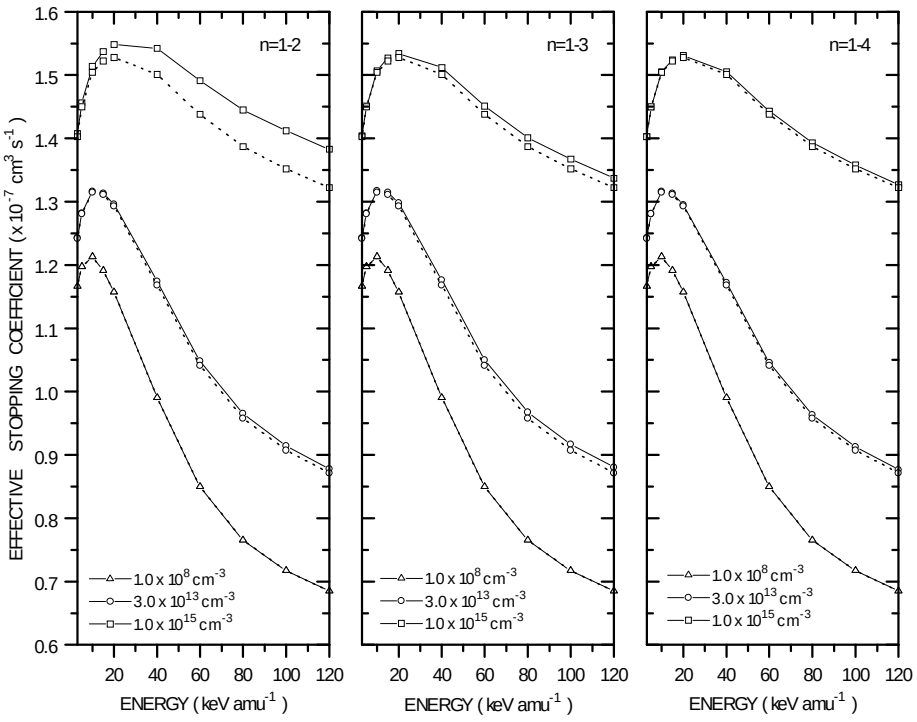

Figure 4.14 Effective stopping coefficient Vs the neutral beam energy for a pure D^+ plasma. Working from left to right the plots illustrate the results of changing the ion impact excitation cross sections from the ground state to the n=2, 3 and n=4 shell. The dashed lines represents the results from the unmodified database. The ion temperature was 2.0 x 10^3 eV and the excitation cross sections were increased by 20%.

Working from left to right, the results of modifying the ion impact excitation cross sections from the ground state to the n=2,3 and n=4 shell can be seen in figure 4.14. The influence of the modified data only becomes important when the electron density is increased. Modifying the excitation cross section for the n=1→2 transition has the most significant effect. A maximum increase in the effective stopping coefficient by 0.96 % at 3.0 x 10^{13}cm^{-3} can be observed, which then increases to 4.54 % at 1.0 x 10^{15} cm^{-3}. This is due to the large ion impact ionisation cross section associated with the n=2 shell, as the n=2 population is enhanced by increasing the n=1→2 excitation cross section, the rate at which electrons are stripped from the beam atoms increases.

The influence of changing the cross sections for charge exchange and ion impact ionisation associated with excited states is now of interest. The ion-atom database contains such data for the n=2,3,4 and n=5 shell. In figure 4.15 the results of increasing all of the cross sections by 30 % can be seen as a function of beam energy for three different electron densities.

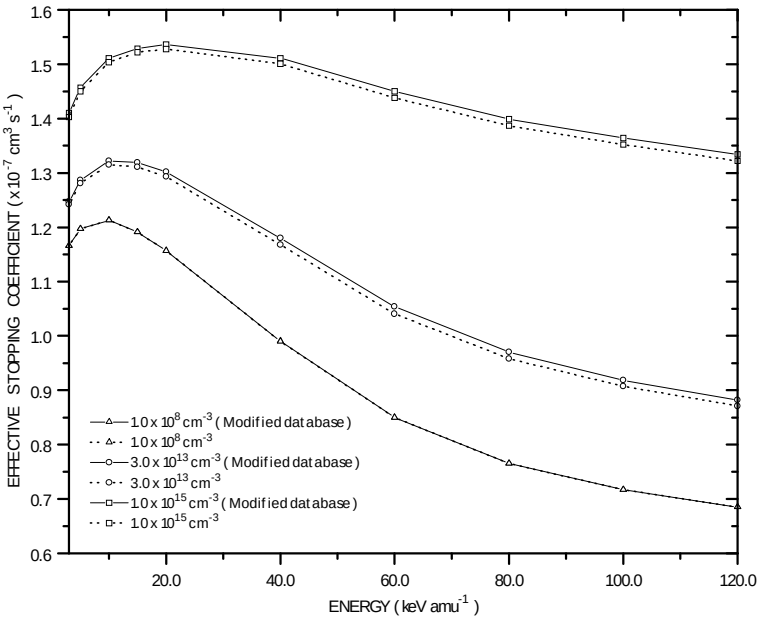

Figure 4.15 Effective stopping coefficient Vs the neutral beam energy for a pure D^+ plasma. The electron densities were selected to correspond to the coronal, collisional-radiative and the high density picture. The ion temperature was 2.0 x 10^3 eV. The charge exchange and ion impact ionisation cross sections associated with the n=2,3,4 and 5 shell were increased by 30 %.

As can be observed, a change in the cross section by 30 % at an electron density of 1.0 x10^{8} cm^{-3} has no effect. Even as the density is increased the effect is minimum. This is due to the fact that the excited state populations are very small. A maximum difference of 1.26 % at 1.0 x 10^{15} cm^{-3} can be observed. In figure 4.16 we show the results of separately modifying the charge exchange and ion impact ionisation cross section by 30%.

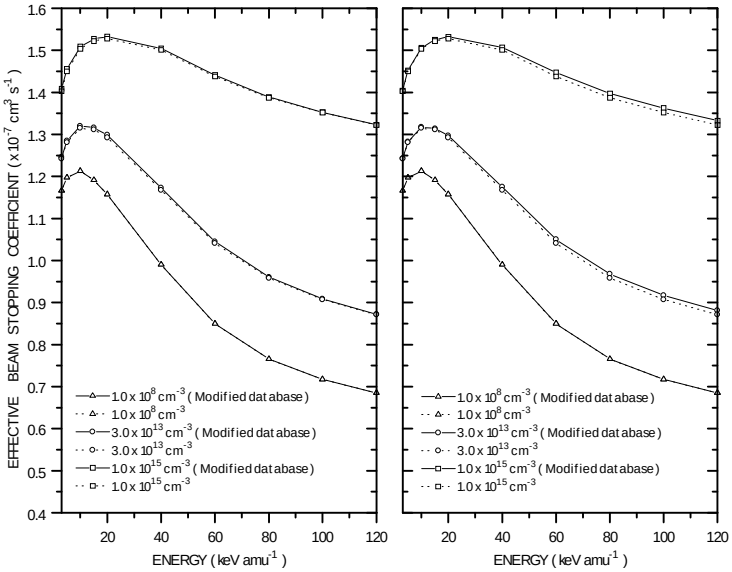

Figure 4.16 Effective stopping coefficient Vs the neutral beam energy for a pure D^{+} plasma. The figure on the left illustrates the results of increasing the charge exchange cross sections associated with the excited states (n=2,3,4 and 5 shell) by 30 %. The plot on the right shows the behaviour of altering the ion impact ionisation cross sections also associated with the excited states (n=2,3,4 and 5 shell) by 30 %.

4.2.7 Conclusion

A collisional-radiative treatment is necessary to evaluate the effective stopping coefficients. The coronal picture leads to errors at the operating densities of current tokamaks (~3.0 x10^{13} cm^{-3}), see figure 4.2.

The neutral beam energy governs which atomic process are primarily responsible for the attenuation of the neutral beam atoms, see chapter 2.0.

The plasma temperature influences the relative collision velocity between the beam atoms and the thermal plasma ions. This contributes to either increasing or

decreasing the effective stopping coefficient. The influence of the temperature on the effective stopping coefficient is considerably weaker than the electron density and the neutral beam energy, see figure 4.5. A difference of approximately 12% can be observed when the temperature is changed by a factor of 5.

The nuclear charge of fully stripped plasma ion characterises how effective the ion will be at stripping the electrons from the beam atoms. We have shown that as the nuclear charge of a plasma impurity ion increases, the more effective the ion becomes at ionising the beam atoms.

The role of impurities contained in the plasma has also been shown to be of great importance while evaluating effective stopping coefficients. From the examples that we considered, the contribution to the total stopping coefficients due to each of the impurity ions can be substantial. For a basic plasma consisting of 98% D^+ and 2% He^{2+}, the contribution to the total stopping coefficient due to the He^{2+} ions ranged from 2.5 to 5.69 %. In the case of a more detailed plasma consisting of 93% D^+, 2% He^{2+}, 2% Be^{4+} and 3% C^{6+}, the C^{6+} ions alone contributed up to 27.73 % to the total stopping coefficient.

The influence of the fundamental atomic data on the effective stopping coefficients was investigated. A 10 % increase in the cross sections for direct charge exchange and ion impact ionisation resulted in an increase of approximately 8 % in the stopping coefficient. Stepwise atomic processes counter the influence of direct charge exchange and ion impact ionisation. Increasing the electron density, which enhances stepwise atomic processes, results in reducing the influence of modifying the fundamental data for the direct processes.

Individually increasing the cross sections for each of the direct processes illustrated the energy dependence of their contribution to the stopping coefficient. The contribution due to charge exchange was dominant at the lower energies whilst ion impact ionisation was more significant at the higher energies.

Modifying the ion impact excitation cross sections by 20% had little effect at densities around 1.0×10^8 cm-^{3}. This is due to the fact that at this density the excited states are barely populated. As the density was increased the influence of modifying the excitation cross section was evident. At a density of 3.0×10^{13} cm^{-3} a change in

the excitation cross sections by 20 % resulted in a change in the stopping coefficient by 2.75 %. Even at 1.0 x 10^{15} cm^{-3} a maximum change of 6.81 % could only be observed. Modifying the excitation cross section for the n=1→2 transition had the most significant effect.

The influence of modifying the charge exchange and ion impact ionisation cross sections associated with excited states was negligible. Altering the cross sections by 30 % only resulted in a maximum change of 1.26 % in the stopping coefficient. This again is attributed to the fact that the excited states populations are very small.

4.3 Effective Balmer-alpha emission coefficients

In a similar manner as in section 4.2, we illustrate the main parameter dependencies of the Balmer-alpha effective emission coefficient. The Balmer-alpha effective emission coefficient directly reflects the population of the n=3 shell of the excited beam neutrals. Figure 4.17 illustrates the global behaviour of the emission coefficient for a neutral deuterium beam penetrating into a pure D^+ plasma.

The main parameter dependencies of the Balmer-alpha effective emission coefficient which are considered include the electron density, the neutral beam energy, plasma temperature and the nuclear charge of the impurity ions contained in the plasma. The ion density is also an important parameter but in the present work the effective emission coefficients are also calculated in terms of the electron density with the condition of charge neutrality imposed.

We also concern ourselves here with two additional physics issues. Firstly, we illustrate the influence of the fundamental atomic data, following small changes, on the behaviour of the Balmer-alpha effective emission coefficient. Secondly we show the importance of taking into account the impurity content of the plasma while evaluating effective emission coefficients.

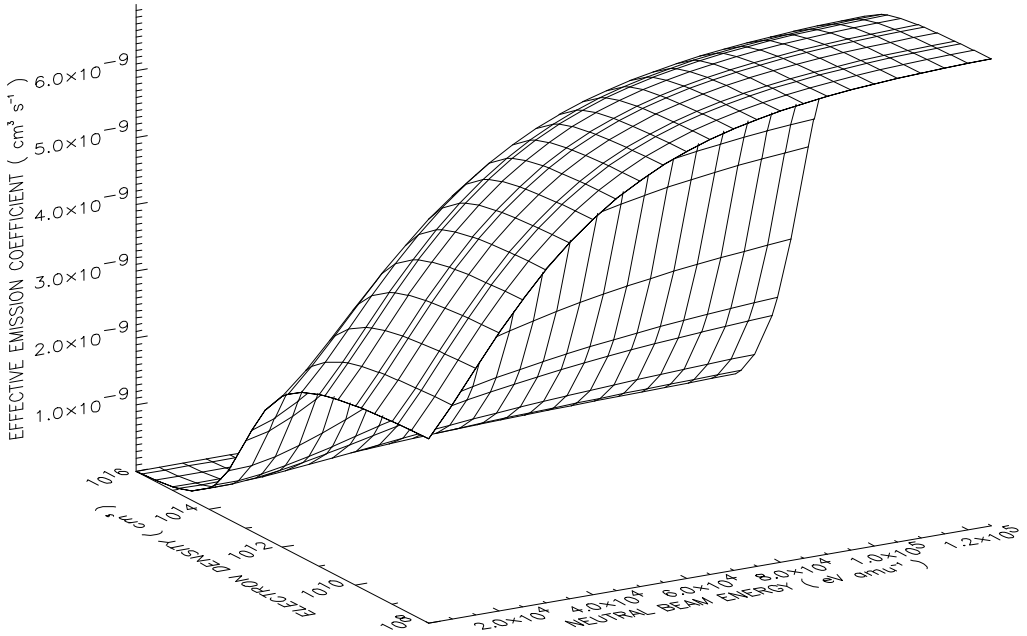

Figure 4.17 A surface plot of the Balmer-alpha emission coefficient for a pure deuterium plasma with a temperature of 2×10^3 eV. The behaviour of the emission coefficient in the coronal limit directly reflects the rate coefficients contributing to populating and depopulating the n = 3 shell. As the density is increased the n = 3 shell becomes considerably depopulated which results in a decrease in the emission coefficient.

4.3.1 Density dependence

The electron and ion density are both responsible for promoting collisional redistribution amongst the excited states of the neutral beam atoms. The latter being of greater influence. We show in figure 4.18 the behaviour of the Balmer-alpha emission coefficient as a function of energy for a range of electron densities.

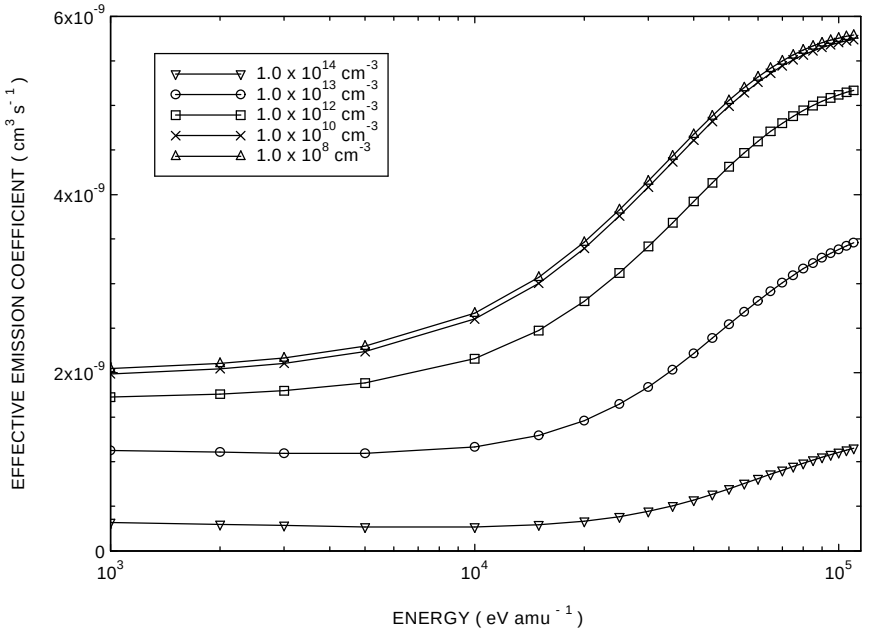

Figure 4.18 Balmer-alpha effective emission coefficient Vs the neutral beam energy for a pure D^+ plasma. The electron density dependence of the effective emission coefficient is clearly illustrated. The plasma temperature was 2.0×10^3 eV

The departure from the low density coronal limit can be observed to occur around $\sim 10^{10}$ cm^{-3} (c.f. figure 4.2). As the electron density is increased, the collisional processes begin to compete with the radiative processes. This results in the n=3 shell also being collisionally depopulated and a decrease in the effective emission coefficient can be observed.

A similar behaviour can be observed when considering plasmas with a different impurity composition. As an example we show in figure 4.19 the density dependence of the effective emission coefficient for a deuterium beam penetrating into a hypothetical C^{6+} plasma. We emphasise, once again, that it is the ion density which is primarily responsible for the collisional redistribution. As mentioned before, the effective emission coefficients in this work are calculated in terms of the electron density.

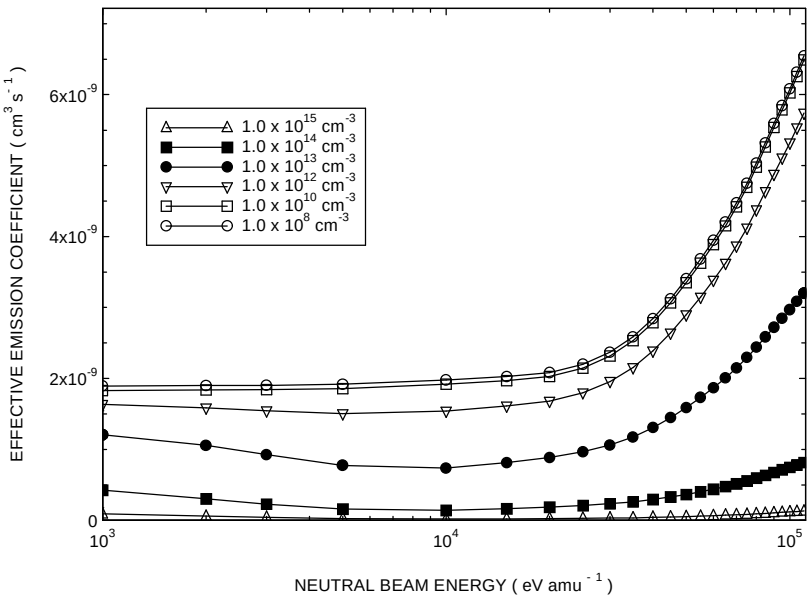

Figure 4.19 Effective emission coefficients Vs the neutral beam energy for a pure C^{6+} plasma. The plasma temperature was 2.0 x 10^3 eV. The coefficient has been calculated in terms of the electron density with the condition of charge neutrality imposed.

It is of interest to point out that in the low energy regime of figures 4.18 and 4.19, the magnitude of the effective emission coefficients are comparable. This is due to the fact that in this regime, electron collisions are primarily responsible for populating the n=3 shell. However as the beam energy increases, the role of the ion collisions become important and the results in each figure begin to differ due to the influence of the nuclear charge associated with each ion. The nuclear charge of the plasma impurity ion determines how effective the ion will be at depopulating the n=3 shell and is discussed in section 4.3.4.

4.3.2 Neutral beam energy dependence

The neutral beam energy controls the efficiency of the fundamental atomic processes which contribute to populating and depopulating the n=3 shell. We show in figure 4.20 the behaviour of the Balmer-alpha effective emission coefficient as a function of electron density for a range of beam energies.

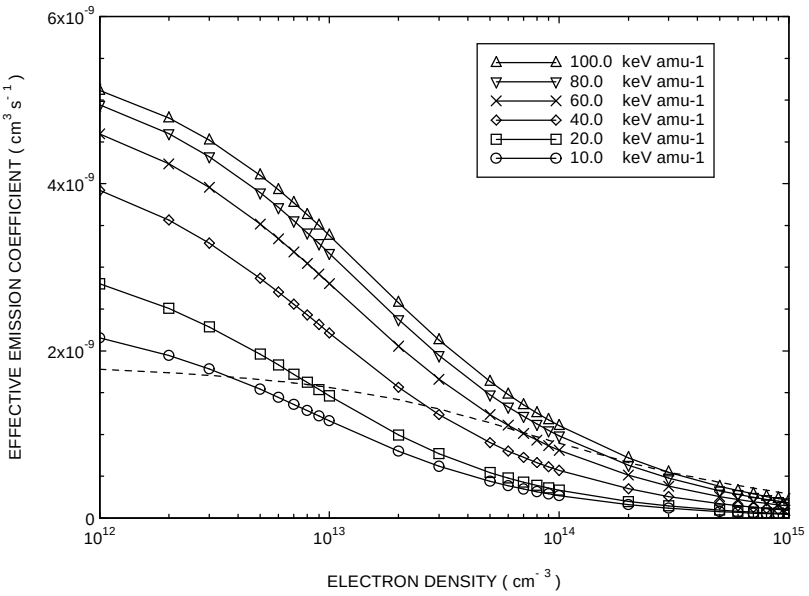

Figure 4.20 The Balmer-alpha effective emission coefficients Vs the electron density for a pure D^+ plasma with a temperature of 2.0 x 10^3 eV. The energy dependence of the Balmer-alpha emission coefficient is clearly illustrated. Also shown, with the dashed lines, is the contribution to the effective stopping coefficient due to electron collisions.

At a density of 1.0 x 10^{12} cm^{-3}, an increase in the beam energy results in an increase in the effective emission coefficient. This simply reflects the energy dependence of the underlying atomic processes which contribute to populating the n=3 shell. In the low energy regime, collisional excitation by electrons is the dominant process. As the neutral beam energy is increased, ion impact excitation, which is more efficient, becomes substantial, see chapter 2.0. It can also be observed that as the electron density is increased the effective emission coefficient decreases. This can be attributed to the influence of stepwise atomic processes, particularly charge exchange and ion impact ionisation from the n=3 shell. Also shown in the figure, with the dashed line, is the contribution to the Balmer-alpha emission coefficient due to electron collisions. This also exhibits a decrease as the electron density is increased.

4.3.3 Temperature dependence

The plasma temperature dependence of the effective emission coefficient also exhibits the same behaviour as shown for the effective stopping coefficients, see

section 4.2.3. In summary, when the beam velocity is slightly greater than the thermal velocity of the plasma ions, an increase in the plasma temperature results in a decrease the relative collision velocity. This in turn may lead to either an increase or decrease in the collision cross sections for the processes which populate the n=3 shell. Where as when the thermal velocity of the ions is slightly greater than the beam velocity, an increase in the temperature results in an increase in the relative collision velocity. In figure 4.21 we show the temperature dependence of the Balmer-alpha emission coefficient as a function of beam energy.

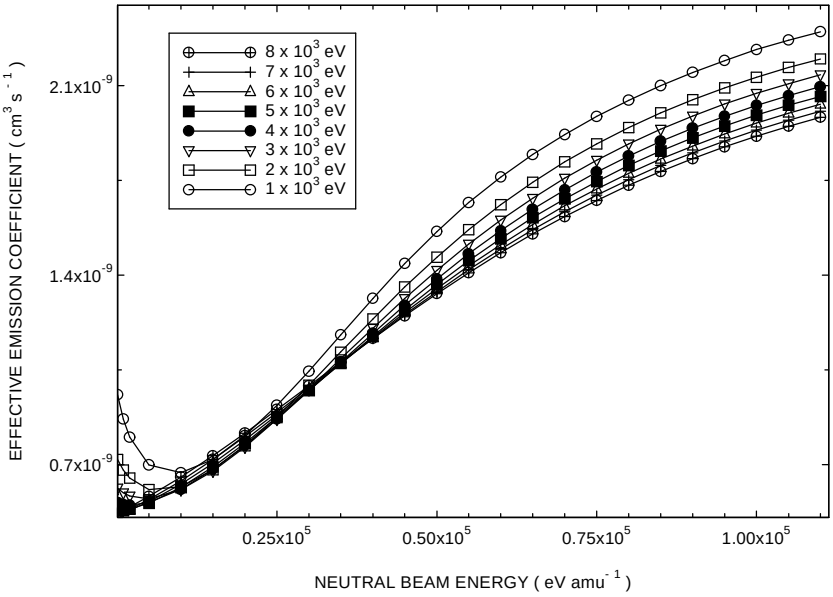

Figure 4.21 Effective Balmer-alpha emission coefficient Vs neutral beam energy for a D^+ plasma . The electron density and plasma temperature was 3.0 x 10^{13} cm^{-3} and 2.0 x 10^3 eV respectively. A change in the effective coefficient by 6.8 % at a beam energy of 30 keV amu^{-1} can be achieved by modifying the temperature by a factor of 5, this increases to 12.7 % at 70 keV amu^{-1}.

As shown in figure 4.21, in the low energy regime an increase in the plasma temperature gives rise to an increase in the effective emission coefficient. This is simply due to an increase in the collision cross sections as a result of increasing the relative collision velocity between the beam atoms and the thermal plasma ions. In the high energy regime the opposite can be observed. It can also be seen that at an energy of 30 keV amu^{-1}, a change in the emission coefficient of 6.8 % can be

achieved by modifying the temperature by a factor of 5. This increases to 12.7 % at 70 keV amu^{-1}. A point to note however is that below 10 keV amu^{-1} a change of up to 40 % can be observed. The temperature dependence of the emission coefficient is larger than that for the effective stopping coefficient. This is due to the increased role of electron collisions which contribute to populating the n=3 shell, see figure 4.20, where as for the effective stopping coefficients, the contribution due to the electrons is very small, see figure 4.4

4.3.4 Nuclear charge dependence

As discussed in 4.2.4, the nuclear charge of a fully stripped plasma ion governs how effective the ion will be at stripping the electrons from the beam atoms. The nuclear charge also determines the extent to which the ion will contribute to the collisional redistribution of the excited states of the beam atoms. In general, the efficiency of the ion increases with nuclear charge. If we consider the population of the n=3 shell, as the nuclear charge of the plasma ion increases, the cross sections for the collisional processes which populate the n=3 shell, such as excitation, also increase. We would then expect the n=3 shell population and hence the Balmer-alpha coefficient to increase. However the cross sections for ion impact ionisation and charge exchange from the n=3 shell also become larger. The net effect is that the population of the n=3 shell becomes smaller as the nuclear charge of the plasma ion increases. We show in figure 4.22, the behaviour of the Balmer-alpha effective emission coefficient as a function of beam energy for a range of pure impurity plasmas.

In the low energy regime the n=3 shell is populated primarily by electron collisions and the Balmer-alpha emission coefficient is almost independent of the beam energy, see figure 4.22. There is a small thermal contribution from each ion, which gives rise to the nuclear charge dependence of the effective emission coefficient. As the beam energy is increased the ion collisions become important and as can be observed the larger the nuclear charge the smaller the effective emission coefficient. We highlight here that the electron density was fixed at 3.0×10^{13} cm^{-3} and charge neutrality was imposed. Therefore as the nuclear charge of the impurity ion increases the corresponding number density decreases.

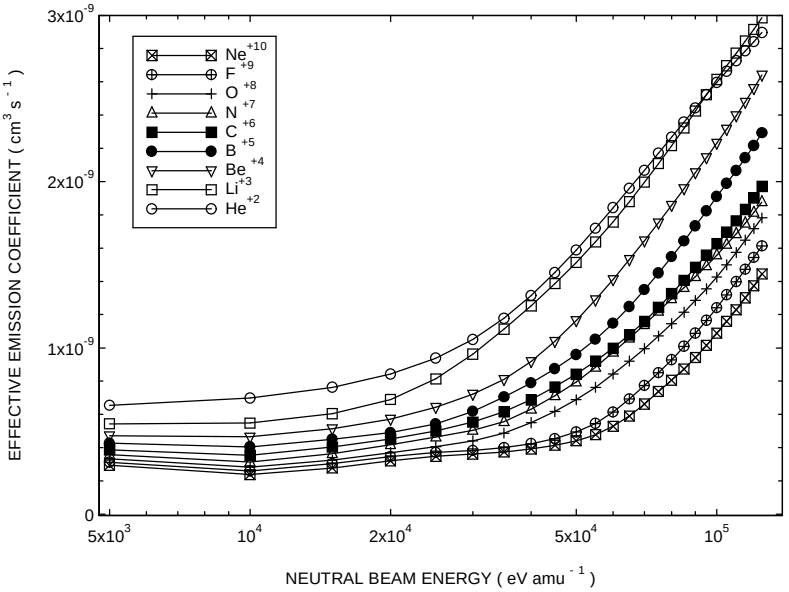

Figure 4.22 Effective emission coefficient Vs neutral beam energy for a range of pure impurity plasmas. The electron density and the plasma temperature was respectively 3.0 x 10^{13} cm^{-3} and 2.0 x 10^3 eV. A point to note is that charge neutrality has been imposed, therefore the number density of impurity ions decreases as the nuclear charge of the impurity species increases.

4.3.5 The importance of impurities

In fusion plasmas, the typical concentration of each impurity ion rarely exceeds 5 %. To simplify the evaluation of the effective emission coefficient, it may then appear to be valid to neglect the impurity content of the plasma. However this is not the case. In this section we illustrate the importance of taking the impurity content of the plasma into account while evaluating effective emission coefficients. The approach adopted here is similar to that of section 4.2.5, here we calculate the effective Balmer-alpha emission coefficient for a range of composite plasmas and in each case illustrate the contribution due to each impurity ion. This will allows us to quantitatively assess the implications of neglecting the impurity content of the plasma while evaluating effective emission coefficients.

We first begin with a composite plasma which consists of 98 % D^+ and 2 % He^{2+}. The energy and density dependence of the composite emission coefficient is shown in figure 4.23. Also shown are the individual contributions due to the D^+ and He^{2+} ions.

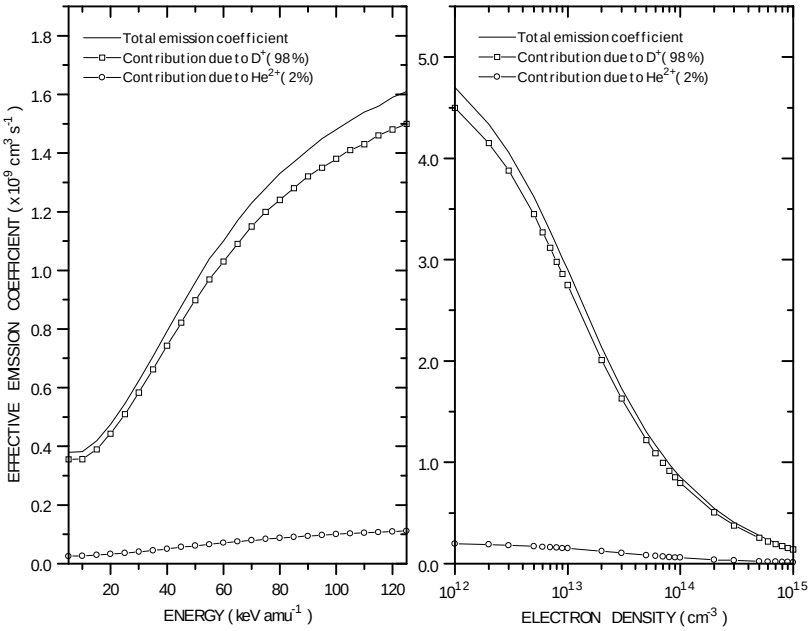

Figure 4.23 A plot of the Balmer-alpha effective emission coefficient for a composite plasma consisting of 98% D^+ and 2% He^{2+}. The plot on the left illustrates the energy dependence of the composite stopping coefficient, while the plot on the right shows the corresponding density dependence.

The energy dependence of the effective emission coefficient is shown in the plot on the left in figure 4.23. It can be observed that the contribution to the total emission coefficient due to the 2% concentration of He^{2+} ions, increases from 6.6 % at 5.0 keV amu^{-1} to 6.95 % at 125 keV amu^{-1}. A similar result can be observed in the plot on the right in figure 4.23, which illustrates the electron density dependence of the emission coefficient. As the electron density is increased the contribution to the composite emission coefficient slowly increases. At a density of 1.0 x 10^{12} cm^{-3}, the contribution due to the He^{2+} ions is 4.14 %, which then increases to a maximum value of 8.70 % at a density of 1.0 x 10^{15} cm^{-3}.

We now consider a slightly different plasma which consists of 96 % D^+, 2% He^{2+} and 2% Be^{4+}. The energy and density dependence of the composite coefficient can be seen in figure 4.24.

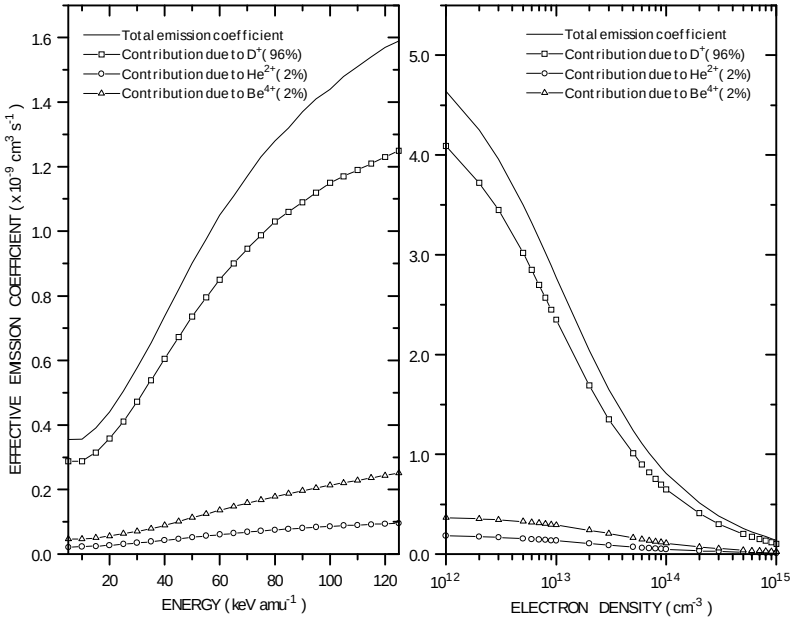

Figure 4.24 A plot of the Balmer-alpha effective emission coefficient for a composite plasma consisting of 96 % D^+, 2 % He^{2+} and 2% Be^{4+} . The plot on the left exhibits the energy dependence of the composite emission coefficient, while the plot on the right illustrates the density dependence. Also shown are the individual contributions due to each ion.

The plot on the left illustrates the energy dependence of the emission coefficient. The individual contributions due to the He^{2+} and Be^{4+} ions respectively increase from 5.97 and 13.12 % at 5.0 keV amu^{-1} to 6.03 and 15.78 % at 125 keV amu^{-1}. The contribution from the Be^{4+} ions is greater since the associated cross sections are larger. In figure 4.24 we also show the electron density dependence of the composite emission coefficient. At a density of 1.0 x 10^{12} cm^{-3}, the contribution due to He^{2+} and Be^{4+} ions are respectively 3.94 and 7.82%. These increase to a maximum value of 8.02 and 16.78 % at a density of 1.0 x 10^{15} cm^{-3}.

The last plasma which we consider consists of 93% D^+, 2 % He^{2+}, 2% Be^{4+} and 3% C^{6+}, see figure 4.25.

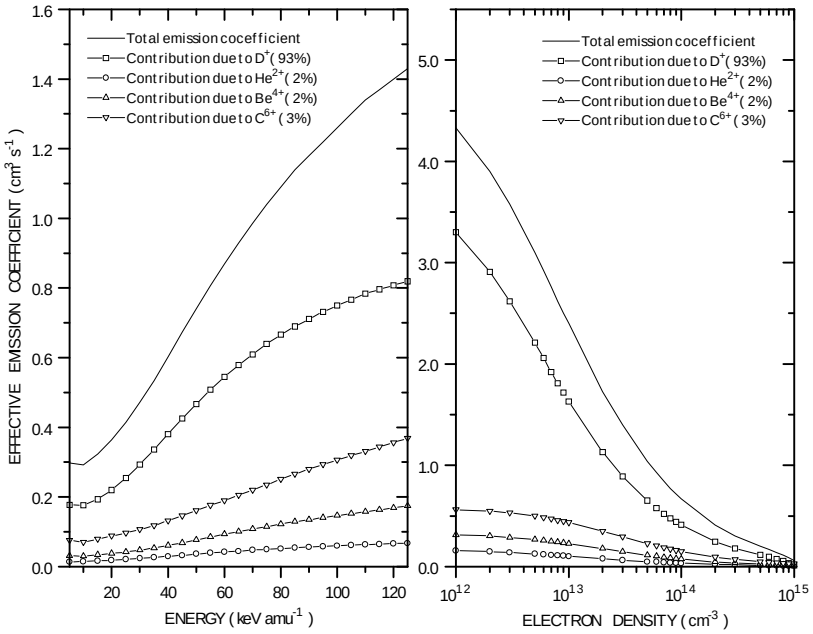

Figure 4.25 A plot of the Balmer-alpha effective emission coefficient for a composite plasma consisting of 93 % D^{+}, 2% He^{2+}, 2% Be^{4+} and 3% C^{6+}. The plot on the left shows the energy dependence of the emission coefficient. The plot on the right illustrates the density dependence. The ion temperature was 2.0 x 10^{3} eV.

The plot on the left exhibits the energy dependence of the coefficient while the plot on the right illustrate the corresponding density dependence. If we confine ourselves with the energy dependence of the effective emission coefficient. It can be observed that the contribution to the total emission coefficient due to the impurity ions increases as a function of energy. At 5.0 keV amu^{-1} the contribution due to He^{2+}, Be^{4+} and the C^{6+} ions are respectively 4.73, 10.43 and 25.26 %. We now consider the electron density dependence of the composite emission coefficient. It can be observed that at a density of 3.0 x 10^{13} cm^{-3}, which is typical the operating density of present day tokamak devices, the contribution due to the He^{2+}, Be^{4+} and the C^{6+} ions are respectively 4.6, 10.5 and 21.07 %. A total combined contribution to the effective emission coefficient due to the impurity ions is ~ 36%.

4.3.6 Influence of fundamental low level data

In this sub-section we investigate the influence of the fundamental atomic data on the effective Balmer-alpha emission coefficient. The approach adopted is similar to that of section 4.2.6, where we individually modify the cross sections associated with each atomic process for a pure D^+ plasma.

We begin by considering the implications of increasing the cross sections for direct charge exchange and ion impact ionisation by 10 %. The results are shown in figure 4.26 as a function of beam energy for three different electron densities.

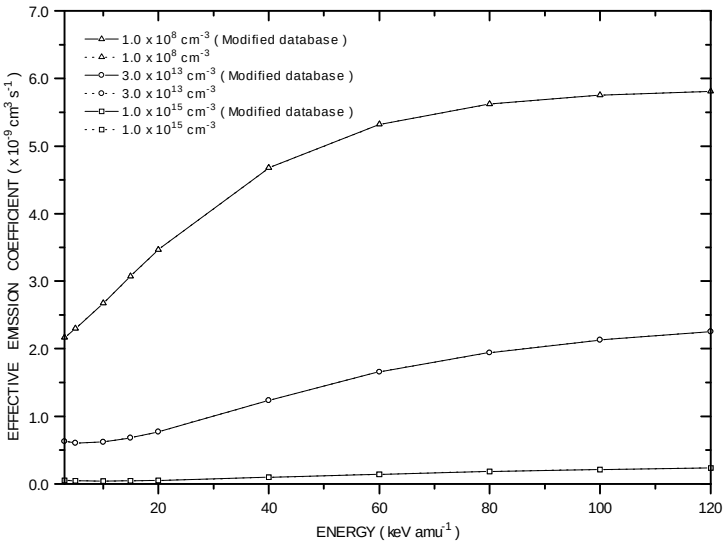

Figure 4.26 A plot of the effective emission coefficient for a pure D^+ plasma. The three densities have been selected to correspond to the coronal, collisional-radiative and the high density picture. The solid lines show the results obtained by increasing the direct charge exchange and ion impact ionisation cross sections by 10 %. The ion temperature was 2 x 10^3 eV.

As can be observed, increasing the direct charge exchange and ion impact ionisation cross sections has a negligible effect. This is such a contrast to the behaviour of the effective stopping coefficients. Earlier we saw that such a change in the fundamental data gave rise to an increase of approximately 8 % in the effective stopping coefficient.

The influence of the ion impact excitation cross sections is now of interest. The ion-atom collision database contains excitation cross sections from the ground

state to the n=2,3,4 and n=5 shell. In figure 4.27 we show the results of increasing all of the excitation cross sections by 20 %, the dashed lines are the results obtained from the unmodified database.

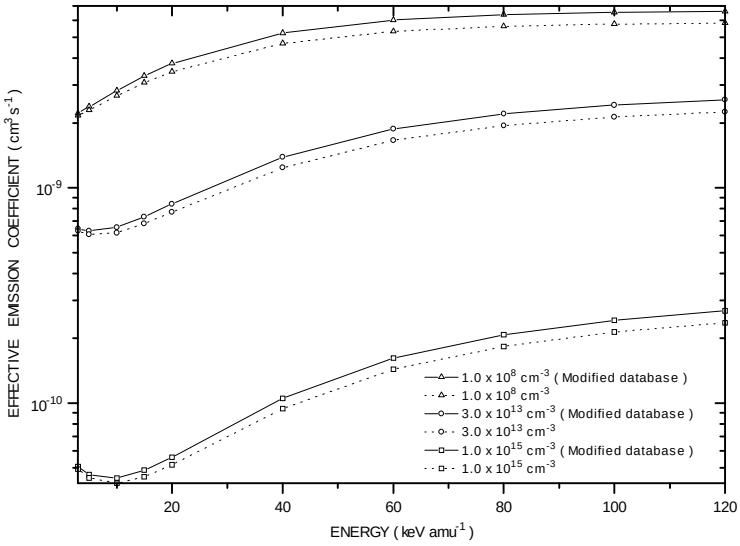

Figure 4.27 A plot of the effective emission coefficient for a pure D^+ plasma. The solid lines illustrate the results obtained by increasing all of the ion impact excitation cross sections by 20%. The dashed lines correspond to the results obtained from the unmodified database. The plasma temperature was 2.0 x 10^3 eV.

It can be observed that the influence of the modified data increases as a function of beam energy and electron density. At 1.0 x 10^8 cm^{-3}, the 20 % increase in the excitation cross sections has given rise to an increase in the emission coefficient by 2.30 % at 3.0 keV amu^{-1}, which then increases to a maximum value of 13.42 % at 120 keV amu^{-1}. As the electron density is increased, the influence of the modified data is slightly enhanced. At 1.0 x 10^{15} cm^{-3} the effective emission coefficient increases from 2.83 % at 3.0 keV amu^{-1} to 13.55 % at 120 keV amu^{-1}.

It is of interest to identify which excitation rate is primarily responsible for influencing the effective emission coefficient. In figure 4.28 we show the results of individually increasing each of the ion impact excitation cross sections by 20 %.

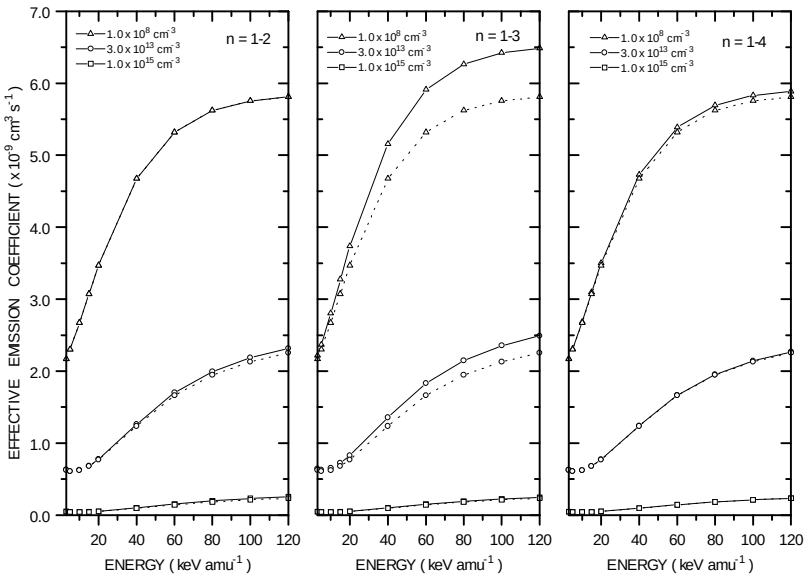

Figure 4.28 A plot of the effective emission coefficient for a pure D^+ plasma. The solid lines indicate the results obtained from modifying the fundamental data, while the dashed lines show the results from the unmodified database. Working from left to right are the results obtained by increasing the excitation cross sections from the ground state to the n=2,3 and n=4 shell by 20%. The plasma temperature was 2.0 x 10^3 eV.

The results of increasing the excitation cross sections associated with the ground state to the n=2,3 and n=4 shell can be observed. The dashed lines represent the results obtained from the unmodified database. Modifying the collisional excitation cross section for the n=1→3 transition has the greatest influence on the effective emission coefficient. At a density of 3.0 x 10^{13} cm^{-3}, an increase of 20 % in this cross section results in the emission coefficient increasing from 2.38 % at 3.0 keV amu^{-1} to 10.66 % at 120.0 keV amu^{-1}. It is worth noting that the influence of the cross section for the n=1→3 transition was very small on the behaviour of the stopping coefficient, the most influential data was that associated with the n=1→2 transition.

We now investigate the influence of the fundamental data which describes charge exchange and ion impact ionisation associated with the excited states. The ion-atom collision database contains such data for the n=2,3,4 and n=5 shell. In figure 4.29, we show the results of increasing all of the charge exchange and ion impact ionisation cross sections by 30%.

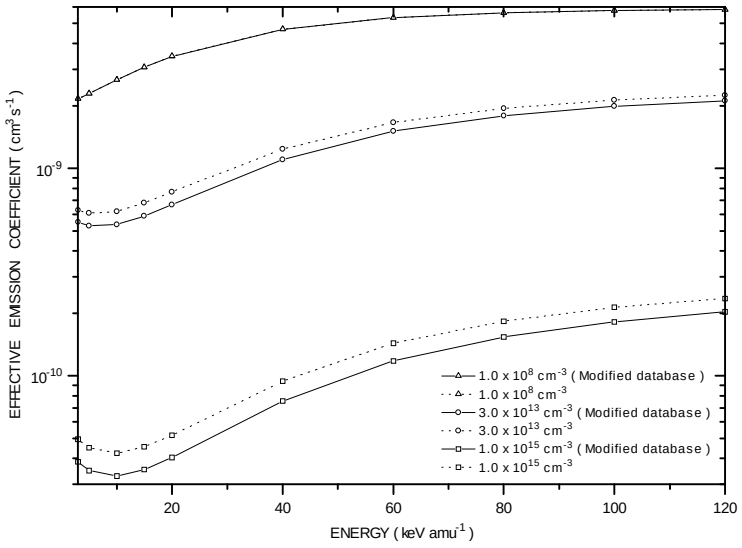

Figure 4.29 A plot of the effective emission coefficient for a pure D^+ plasma. The solid lines show the results obtained by increasing the cross sections for charge exchange and ion impact ionisation associated with the excited states by 30 %. The dashed lines are the results from the unmodified database.

At 1.0 x 10^8 cm^{-3}, increasing the excited state cross sections has little effect. This is due to the fact that at such low densities the excited states are scarcely populated. As the electron density is increased, the excited state populations begin to increase and the influence of the excited state cross sections becomes important. Generally speaking, an increase in the charge exchange and ion impact ionisation cross sections associated with the excited states gives rise to a decrease in the emission coefficient. From figure 4.29 , it can be observed that at an electron density of 1.0 x 10^{15} cm^{-3} , the effective emission coefficient decreases by 21.8 % at 3.0 keV amu^{-1}. The influence of the modified data becomes less as the beam energy increases, at 120 keV amu^{-1} a difference of 13.98 % can be observed. Interestingly though, the influence of such data on the effective stopping coefficients was negligible.

In figure 4.30 we show the results of individually increasing the charge exchange and ion impact ionisation cross sections associated with the excited states by 30 %.

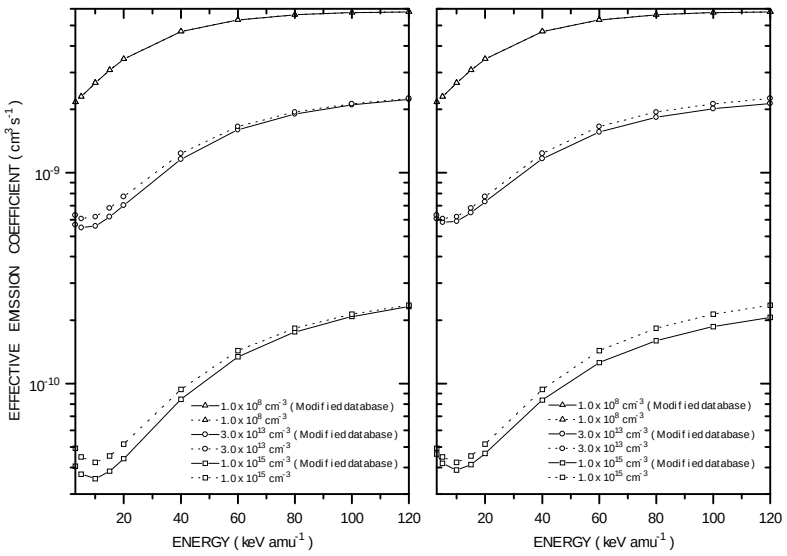

Figure 4.30 A plot of the effective emission coefficient for a pure D^+ plasma. The plot on the left illustrates the results of increasing all of the charge exchange cross sections associated with the excited states by 30 %. The plot on the right shows the influence of increasing the ion impact ionisation cross sections associated with the excited states by 30 %. The solid lines are the results from the modified database. The dashed lines are the results from the unmodified database.

If we consider the plot on the left, which shows the results of increasing the charge exchange cross sections associated with the excited states. It can be observed that as the beam energy increases, the reduction in the effective emission coefficient decreases. This simply reflects the energy dependence of the charge exchange cross sections. A similar type of behaviour can be observed on the plot on the right, which illustrates the results of changing the ion impact ionisation cross sections. However in this case, the decrease in the effective emission coefficient increases as function of beam energy.

4.3.7 Conclusion

At the operating densities of current tokamaks, a collisional-radiative treatment is also required to evaluate the effective emission coefficients, see figure 4.18.

The neutral beam energy determines the efficiency of the atomic processes which contribute to populating the n=3 shell. Electron impact excitation is the

dominant process in the low energy regime, as the energy is increased ion collision become important, see chapter 2.0.

A change in the plasma temperature alters the relative collision velocity between the beam atoms and the plasma ions. This gives rise to either an increase or decrease in the effective emission coefficient.

The temperature dependence of the effective emission coefficient is greater than that for the effective stopping coefficients. This is due to the increased role of electron collisions which contribute to populating the n=3 shell, see figure 4.20.

The nuclear charge of a fully stripped plasma impurity ion governs the effectiveness at which the ion contributes to depopulating the n=3 shell. For a fixed electron density, as the nuclear charge of the impurity ion increases, the Balmer-alpha effective emission coefficient decreases.

We explored the implications of neglecting the impurity content of a plasma while evaluating effective emission coefficients. From the composite plasmas that we considered, we found that each plasma impurity ion contributes substantially to the effective emission coefficient. For a composite plasma consisting of 96% D^+, 2% He^{2+} and 2% Be^{4+}, the minimum contribution to the emission coefficient from each impurity ion was respectively 3.94 and 7.82 %. Even for a plasma consisting of 93 % D^+, 2% He^{2+}, 2% Be^{4+} and 3% C^{6+}, the combined contribution to the emission coefficient due to all of the impurity ions was as much as ~ 36 %.

The influence of the fundamental data on the behaviour of the emission coefficient was investigated. Increasing the cross sections for direct charge exchange and ion impact ionisation by 10 % had a negligible effect. This is such a contrast to the behaviour of the effective stopping coefficients, see section 4.2.6.

Modifying the ion impact excitation cross sections gave rise to a maximum increase in the effective emission coefficient of 13.55 % . The cross section for the $n=1\rightarrow3$ transition had the greatest influence on the Balmer-alpha emission coefficient. Increasing this cross section by 20% gave rise to an increase in the effective emission which ranged from 2.28 % at 3.0 keV amu^{-1} to 10.66 % at 120 keV amu^{-1}. It is of interest to point out here that the excitation cross section for the $n=1\rightarrow3$ transition had little effect on the stopping coefficient.

The influence of charge exchange and ion impact ionisation associated with the excited states was studied. Increasing the cross sections for these processes resulted in decreasing the effective emission coefficient. This was simply due to the fact that charge exchange and ion impact ionisation associated with the excited states contributes to depopulating the n=3 shell.

4.4 Application to experimental programs

4.4.1 Introduction

As discussed earlier, there are two methods which may be employed to determine the neutral beam density at points along the beam line. A numerical attenuation calculation and an experimental spectroscopic method. The latter involves measuring the intensity of the D-α light emitted from the excited beam neutrals and is formally known as beam emission spectroscopy, see chapter 5.0. The effective beam stopping coefficients are employed in the attenuation calculation, whilst the effective Balmer-alpha emission coefficients are used to recover the neutral beam density via beam emission spectroscopy. To satisfy the demands of experimental analysis for inter pulse reduction of data and physical parameters, for example at JET, there is a requirement to compute the neutral beam density on a rapid and automatic basis. Therefore ab intio calculations of the effective stopping or emission coefficients for each changed set of plasma conditions in real time are impractical and a method of constructing and storing fast look up tables of the effective coefficients is sought.

In the following sections we discuss the practical production, archiving and application of such fast look up tables. A linear combination and interpolation method for multiple impurity plasmas has been suggested and used by Summers[26]. The effective coefficients for a plasma containing a variety of impurities are assembled from a collection of look up tables. Each separate look up table contains coefficients calculated for a single impurity species. We examine the accuracy of this linear combination and interpolation method.

4.4.2 Production and archiving the derived data

As discussed in detail in chapter 3.0, the calculation of the effective beam stopping and emission coefficients is done using a bundled-nS collisional-radiative model called ADAS310. Using ADAS310, very complete calculations of the excited population structure are in fact performed. The tabulated population structure and the effective stopping coefficients are stored as a function of plasma parameters in the ADAS data format of adf26. The plasma parameters include the neutral beam energy, electron density, the plasma temperature and impurity species mix (multiple or single). To assemble fast look up tables an interactive program, ADAS312, is employed to extract the effective stopping and emission coefficients, this is discussed in chapter 3.0. An overview of the production and storage of the derived data is shown in figure 4.31.

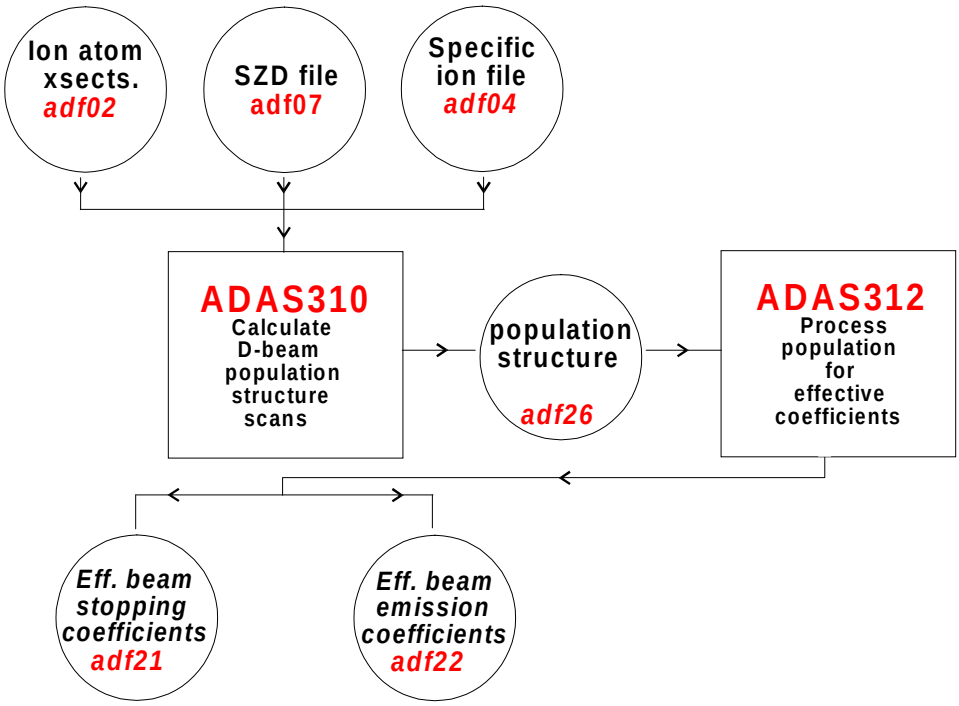

Figure 4.31 Schematic overview of the production of the derived coefficients. Starting with the fundamental data which is used as input for ADAS310. A detailed calculation of the excited population structure and effective stopping coefficients are performed. The output is tabulated in the format of ADAS data type adf26. An interrogation code ADAS312 is then employed to extract the effective stopping and emission coefficients from the adf26 type file.

4.4.3 Linear interpolation scheme

The storage of the derived data in both the adf21 and adf22 type files is designed to economise on the access time of retrieving the stored coefficients. To achieve this the coefficients are stored in a format consisting of a two dimensional scan in energy and density and a one dimensional scan in temperature. Since the temperature dependence of the coefficients is almost independent of the beam energy and density, the one and two dimensional grid can be used to compute the coefficient for any parameter value contained within the tabulated range. The two dimensional scan is achieved by tabulating the coefficients as a function of neutral beam energy and electron density at a fixed reference temperature, while the one dimensional scan is assembled as a function of temperature at fixed reference values for the beam energy and electron density. The schematic in figure 4.32 shows the relationship between the one and two dimensional scan.

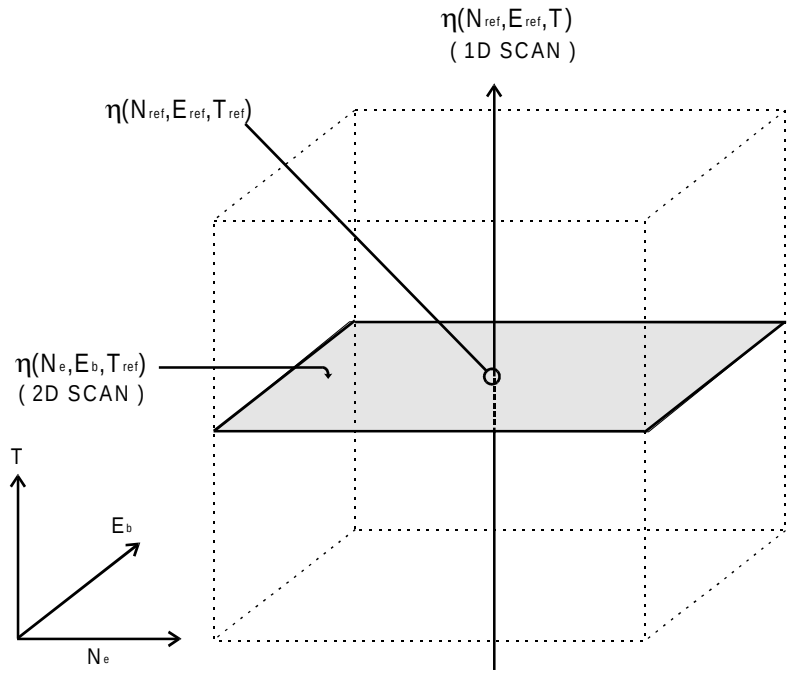

Figure 4.32 Illustration of the one and two dimensional scan employed to create compact data sets. The plasma temperature, neutral beam energy and the electron density are respectively represented using T, E_b and n_e. The subscript 'ref' indicates that the parameter is being treated as a reference value and is held as a constant.

To evaluate the effective coefficient using the one and two dimensional scan the following relation is then employed,

$$\eta(E_b, n_e, T) \approx \left[\frac{\eta(E_b^{REF}, n_e^{REF}, T)}{\eta(E_b^{REF}, n_e^{REF}, T^{REF})} \right] \eta\left(E_b, n_e, T^{REF}\right) \qquad 4.2$$

where η represents either effective beam stopping or emission coefficients. The quantities E_b, n_e and T respectively correspond to the beam energy, electron density and the plasma temperature. The associated superscripts simply indicate the value is employed as a reference.

4.4.4 Linear combination scheme

In designing compact data sets for the storage of the effective coefficients, we now require a method which would allow one to assemble effective coefficients for a plasma contaminated with impurities. The method adopted in this work was first developed by Summers[26] and can be described as a linear combination scheme. The effective coefficient data sets for each fully stripped impurity species up to the first period are calculated as though the species alone is present in the plasma. A linear combination of the individual data sets is then used to synthesis a composite coefficient for a plasma which may contain a variety of impurity species. The combination of the pure impurity data sets is based on the assumption that the contributions from each impurity ion in the plasma are additive. To obtain the total composite coefficient one simply adds the contribution from each impurity species according to there appropriate concentration found in the plasma. In the case of the effective beam stopping coefficients which are calculated in terms of the electron density. The total stopping coefficient for a plasma consisting of n impurities is given as,

$$S_{CR}^{Total}\left(E_b, n_e, T\right) = \sum_{n=1} z_0^n f^{Z_0^n} S_{CR}^{Z_0^n}\left(E_{b,} n_e^{Z_0^n}, T\right) \Big/ \sum_{n=1} z_0^n f^{Z_0^n} \qquad 4.3$$

The quantity n_e^{z0n} is the effective electron density due to the n^{th} impurity and is given by the following expression,

$$n_e^{Z_0^n} = \left[\sum_{n=1} z_0^{n2} f^{Z_0^n} \Big/ \sum_{n=1} z_0^n f^{Z_0^n} \right] \frac{n_e}{z_0^n} \qquad 4.4$$

The effective stopping coefficient due to the n^{th} impurity species is $S_{CR}^{(z0n)}$ and f^{Z0n} is the corresponding fraction contained in the plasma, which is specified in terms of the total electron density, n_e. The beam emission coefficients are handled in the same manner.

An interactive program as well as a selection of FORTRAN routines which implement the linear interpolation and combination method can be found in ADAS. The interactive program, ADAS304[26], is designed to allow one to interactively assemble either effective stopping or emission coefficients for a composite plasma using the pure impurity data sets. The selection of FORTRAN routines enable one to directly implement the linear combination method in an experimental analysis program.

4.4.5 Accuracy of the linear combination and interpolation scheme

In this section we investigate the accuracy of the linear interpolation and combination scheme. This is achieved by simply comparing our results obtained from the true calculation of ADAS310 with the linear methods of ADAS304. We first consider effective beam stopping coefficients and then extend our study to include effective beam emission coefficients. In both cases we have considered a wide range of scenarios but only summarise the main features here.

4.4.5.1 Effective beam stopping coefficients

In the following series of examples we show the percentage difference between the results obtained from the true calculation and the linear combination and interpolation method. It is convenient to consider the accuracy of the linear combination and interpolation method separately. This can be achieved by first studying the assembly of the effective coefficients using a temperature which

corresponds to the reference temperature. Therefore the linear interpolation along the one dimensional temperature grid is suppressed. This allows us to investigate the accuracy of the linear combination method. We can then study the assembly of the effective stopping coefficients under conditions which requires the linear interpolation along the one dimensional temperature grid. This enables us to study the combine accuracy of both linear methods.

The first hypothetical plasma that we consider consist of 75 % D^{+} and 25 % Be^{4+}. The impurity content of the plasma has been exaggerated to illustrate the accuracy of the linear methods under extreme conditions. We show in figure 4.33, as a function of beam energy the accuracy of the linear combination method for a range of electron densities. The plasma temperature has been selected to correspond to the reference temperature

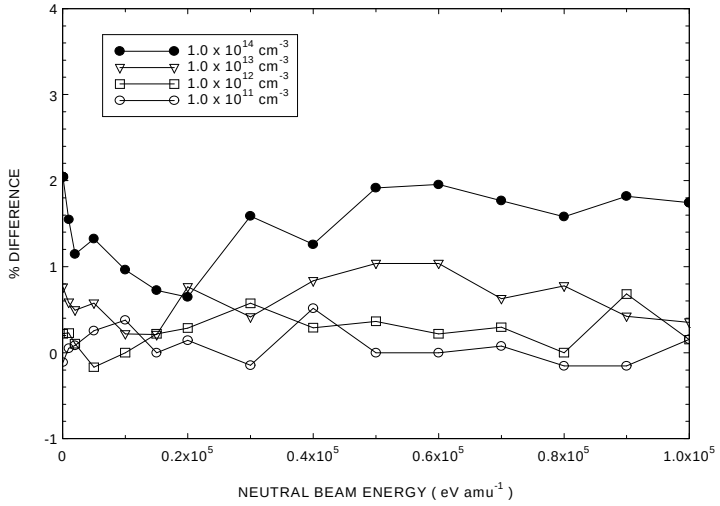

Figure 4.33 A plot of the percentage difference between the output from ADAS304 & ADAS310. The above illustrates that accuracy of the linear assembly performed by ADAS304, a maximum difference of 1.79 % can be observed . The reference density and temperature are respectively 6.78 $\times 10^{10}$ cm^{-3} and 2.0 x 10^{3} eV.

A maximum difference between the results of ADAS310 and ADAS304 of 1.79 % can be observed. We now consider the evaluation of the effective coefficients using both the linear interpolation and combination method. In figure 4.34 we show the

results as a function of energy for a range of temperatures. Therefore interpolation along the temperature grid is required.

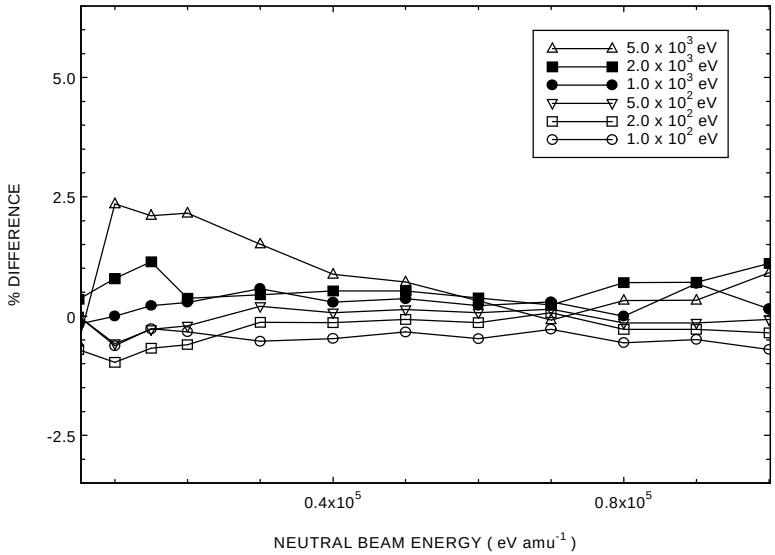

Figure 4.34 A plot of the percentage difference between the output of ADAS304 & ADAS310. Using a reference temperature of 2×10^3 eV , the maximum difference can be observed to be 1.96 %. However below 2×10^3 eV amu^{-1} the difference rises to 2.64 % and continues to reach a peak of 20.70 % at 100 eV amu^{-1} . The electron density was set to a value of 1×10^{12} cm^{-3} and the reference density was 6.78×10^{10} cm^{-3}.

Above 2.0 keV amu^{-1} a maximum difference of 1.96 % can be observed, however below this energy value the difference rises to a peak of 20.70 % at 100 eV amu^{-1}. We now extend our investigation by considering a more complicated plasma. The plasma which is under scrutiny consists of 70% D^+, 20% C^{6+} and 10% Be^{4+}. The accuracy of the linear combination method is first considered, see figure 4.35. A maximum difference of 1.86 % can be observed between the results obtained from ADAS310 and ADAS304. In figure 4.36 we show the accuracy of both the linear interpolation and combination method. Above 2.0 keV amu^{-1} a difference of 2.33 % can be seen. This difference decreases as the beam energy increases. As mentioned earlier, we have undertaken a wide study and a similar accuracy obtained by the linear methods was observed.

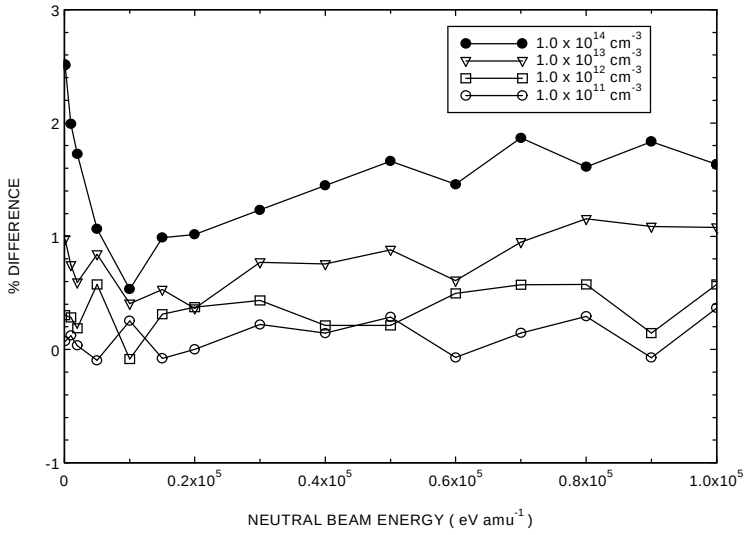

Figure 4.35 A plot of the percentage difference between the output of ADAS304 & ADAS310. The maximum difference seen above is 1.86 %, below 2×10^3 eV amu^{-1} this difference rises to 2.514 %. The electron density was set to a value of 1×10^{12} cm^{-3} and the reference density was 6.78 $\times 10^{10}$ cm^{-3}.

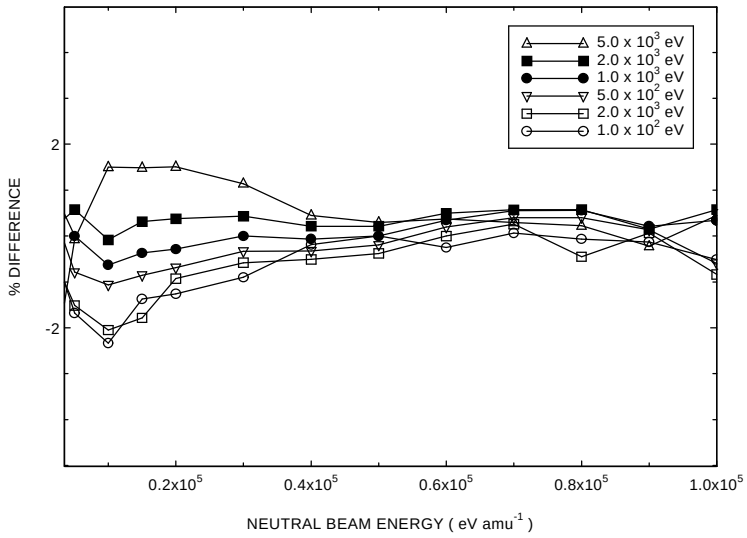

Figure 4.36 A plot of the percentage difference between ADAS304 & ADAS310. Using a reference temperature of 2×10^3 eV, the maximum difference that can be observed is 2.33 %, however below 2×10^3 eV amu^{-1} the difference rises to 5.86 % and continues to reach a value of 23 % at 100 eV amu^{-1}. The electron density was set to a value of 1×10^{12} cm^{-3} and the reference density was 6.78 $\times 10^{10}$ cm^{-3}.

4.4.5.2 Effective beam emission coefficients

We now turn our attention to the accuracy of the linear combination and interpolation method when used to assemble effective emission coefficients for a composite plasma. The approach adopted here is much the same as with the effective stopping coefficients. We first consider the accuracy of the linear combination method and then we study the combined accuracy of both linear methods. It is expected here that the accuracy of the linear methods will be less due to the increased temperature dependence associated with the effective emission coefficient.

We first consider a plasma consisting of 75% D^+ and 25% Be^{4+}. The results can be seen in figure 4.37 as a function of beam energy for a range of densities. The temperature has been selected to correspond to the reference temperature, therefore no interpolation along the temperature grid is required and the results in figure 4.37 simply reflect the accuracy of the linear combination method.

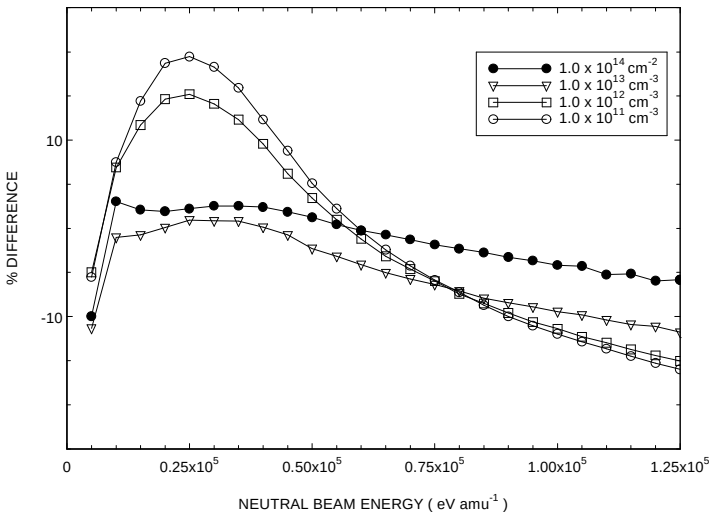

Figure 4.37 Percentage difference between the results from ADAS310 and ADAS304. The temperature was 2.0 x 10^3 eV and the reference values for the beam energy and electron density were respectively 4.0 x 10^4 eV amu^{-1} and 6.78 x 10^{11} cm^{-3}.

At a density and beam energy of 1.0 x 10^{12} cm^{-3} and 25 keV amu^{-1} respectively, a maximum difference of 19.46 % can be observed. We now investigate the combine accuracy of the linear interpolation and combination. In figure 4.38 we show the difference between the results obtained from ADAS310 and ADAS304 as a function

of beam energy for a range of temperatures. In this case, interpolation using the one dimensional temperature grid is required.

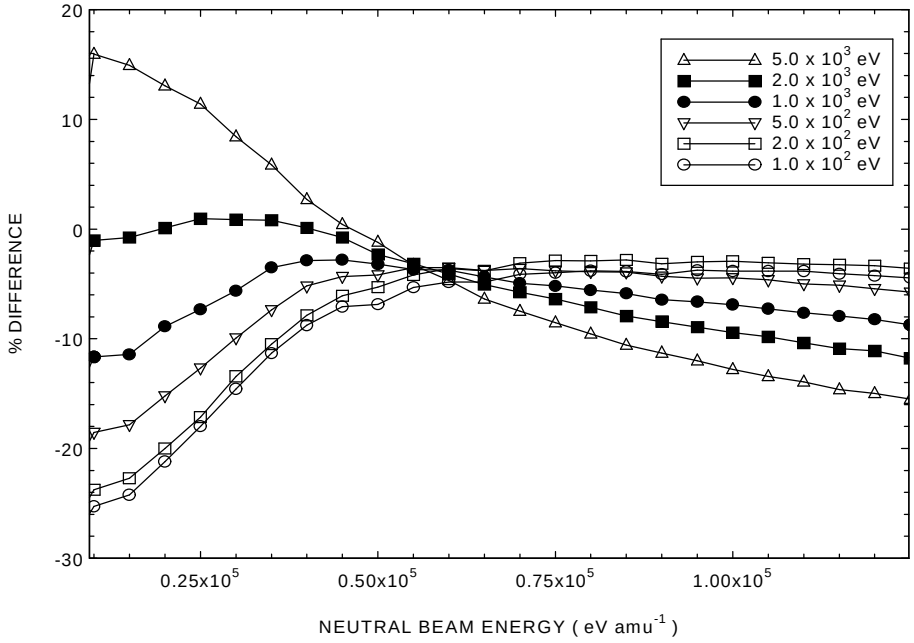

Figure 4.38 Percentage difference between the results obtained by ADAS310 and ADAS304. The reference values for the temperature, beam energy and density were respectively 2.0 x 10^3 eV, 40 keV amu^{-1} and 6.78 x 10^{11} cm^{-3}.

As can be observed, a maximum difference of 25 % occurs at a temperature of 100 eV and a beam energy of 15 keV amu^{-1}. However, this difference decreases as the neutral beam energy increases.

We now extend our study by considering a slightly different plasma. The plasma which is of interest now consists of 70% D^+, 20% C^{6+} and 10% Be^{4+}. In figure 4.39 we show the accuracy of the linear combination method where the temperature has been selected to avoid any interpolation along the temperature grid.

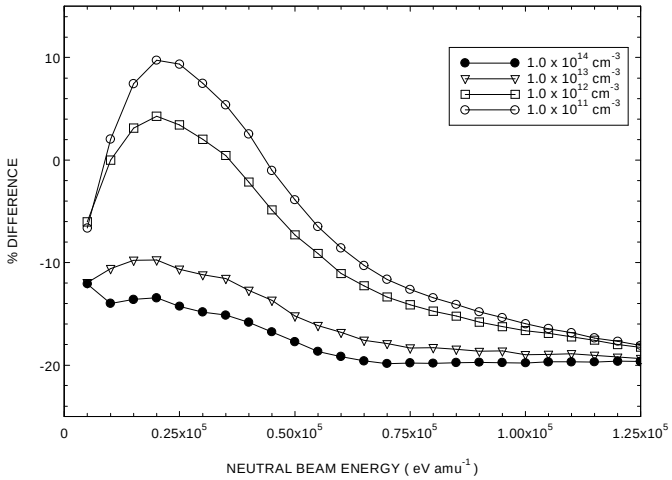

Figure 4.39 Percentage difference between the results obtained from ADAS310 and ADAS304. The composite plasma consist of 70% D^+, 20% C^{6+} and 10% Be^{4+}. The reference values for the temperature, beam energy and density were respectively 2.0 x 10^3 eV, 40 keV amu^{-1} and 6.78 x 10^{11} cm^{-3}.

A maximum difference of 19.86 % at 1.0 x 10^{15} cm^{-3} can be seen. We now show in figure 4.40 the results where the linear interpolation along the one dimensional temperature grid is required.

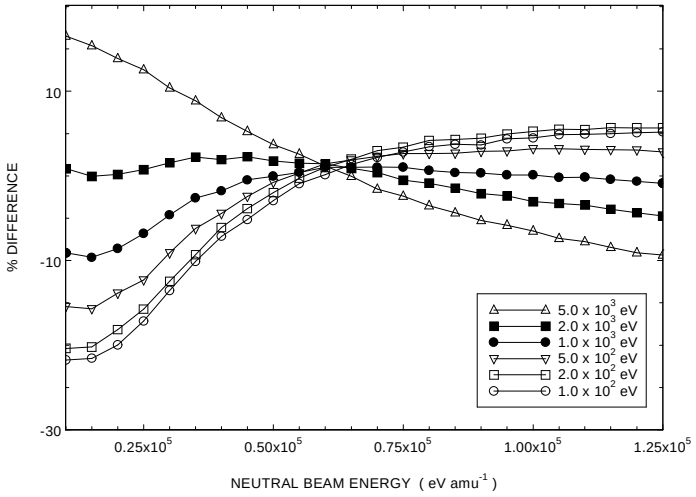

Figure 4.40 Percentage difference between the results obtained by ADAS310 and ADAS304. The reference values for the temperature, beam energy and density were respectively 2.0 x 10^3 eV, 6.67 x 10^{11} cm^{-3} and 40 keV amu^{-1}.

A difference of 21.75 % can be observed at a temperature of 100 eV and similar results can be observed for different composite plasmas.

4.4.6 Conclusion

The creation of compact look up tables enables effective stopping and emission data to be available for routine experimental analysis. The linear combination and interpolation method is successful at assembling effective stopping or emission coefficients for typical composite plasma with speed and reasonable accuracy.

In the case of the effective beam stopping coefficients, the linear combination and interpolation scheme proved to be capable of rapidly assembling composite coefficients which were within 5 % of the values obtained from ADAS310. This level of accuracy however was not retained when we considered the effective emission coefficients. On average, the linear combination and interpolation method could only assemble a composite emission coefficient which was within 20% of the value obtained from the calculation of ADAS310. However this level of accuracy is sufficient for the present application.